Sensors & Diagnostics

PERSPECTIVE

View Article Online
View Journal | View Issue

Cite this: *Sens. Diagn.*, 2024, **3**, 40

Electroanalytical overview: the measurement of ciprofloxacin

Robert D. Crapnell, Prashanth S. Adarakatti and Craig E. Banks *

Ciprofloxacin is a third-generation synthetic fluoroquinolone antibacterial drug which has been used as a broad-spectrum antibiotic to treat a number of bacterial infections. An excessive use or an overdose of ciprofloxacin can result in several adverse effects to humans and therefore its measurement is critical. Electroanalytical based sensors for ciprofloxacin have advantages over laboratory quantification methods, offering cost-effective, rapid, and portable sensing, which are also sensitive and selective. We chart the succession of electroanalytical methodologies directed toward the detection of ciprofloxacin, which starts off with mercury and then turns to using metal oxides, nanomaterials and finally molecular imprinted polymers. Within this perspective, we offer insights into future development in this field for the sensing of ciprofloxacin.

Received 31st May 2023,
Accepted 23rd October 2023

DOI: 10.1039/d3sd00129f

rsc.li/sensors

1. Introduction to ciprofloxacin

Ciprofloxacin, (1-cyclopropyl-6-fluoro-1,4-dihydro-4-oxo-7-(1-piperazinyl)-3-quinoline carboxylic acid, Fig. 1A) is a third-generation synthetic fluoroquinolone antibacterial drug which has been used against a broad spectrum of Gram-negative and Gram-positive bacteria.[1] It can be used for both humans and animals, and it is usually incompletely metabolized and excreted *via* urine and faeces. As shown within Fig. 1A, ciprofloxacin exists in three states in solution: a cationic form (with a protonated amine group in solutions with pH values below 5.90 ± 0.15), an anionic form (with a deprotonated carboxylic acid group in solution with pH values above 8.89 ± 0.11), and a zwitterionic form.[2] It is reported that for ciprofloxacin, more than 75% of the consumed is unmetabolized and excreted into the environment, polluting surface water, groundwater, and drinking water.[3] These pass into wastewater treatment plants

Faculty of Science and Engineering, Manchester Metropolitan University, Chester Street, Manchester M1 5GD, UK. E-mail: c.banks@mmu.ac.uk; Tel: +44 (0)1612471196

Robert D. Crapnell

Robert D. Crapnell achieved both his MChem and PhD from the University of Hull, United Kingdom, respectively, in 2014 and 2018. He is currently a senior research associate at Manchester Metropolitan University, United Kingdom. His research is predominantly focused on fundamental electrochemistry, additive manufacturing, sustainability, bespoke filament production and electrochemical and thermal biosensor development.

Prashanth S. Adarakatti

Prashanth S. Adarakatti did his post-graduation from P. C. Jabin Science College, Hubballi, India. He completed his Doctorate degree in 2017 from Central College, Bangalore University, India. Then he started his postdoctoral studies at the Indian Institute of Science (IISc), Bengaluru, India. He started his career working as an Assistant Professor of Chemistry at SVM Arts, Science and Commerce College, ILKAL, affiliated to Rani Channamma University, Belagavi, Karnataka, India. Currently, he is working as a research associate at Manchester Metropolitan University, Manchester, UK under Prof. Craig E. Banks' supervision. His research focuses on the development of electrochemical sensors and electroanalysis of energy materials.

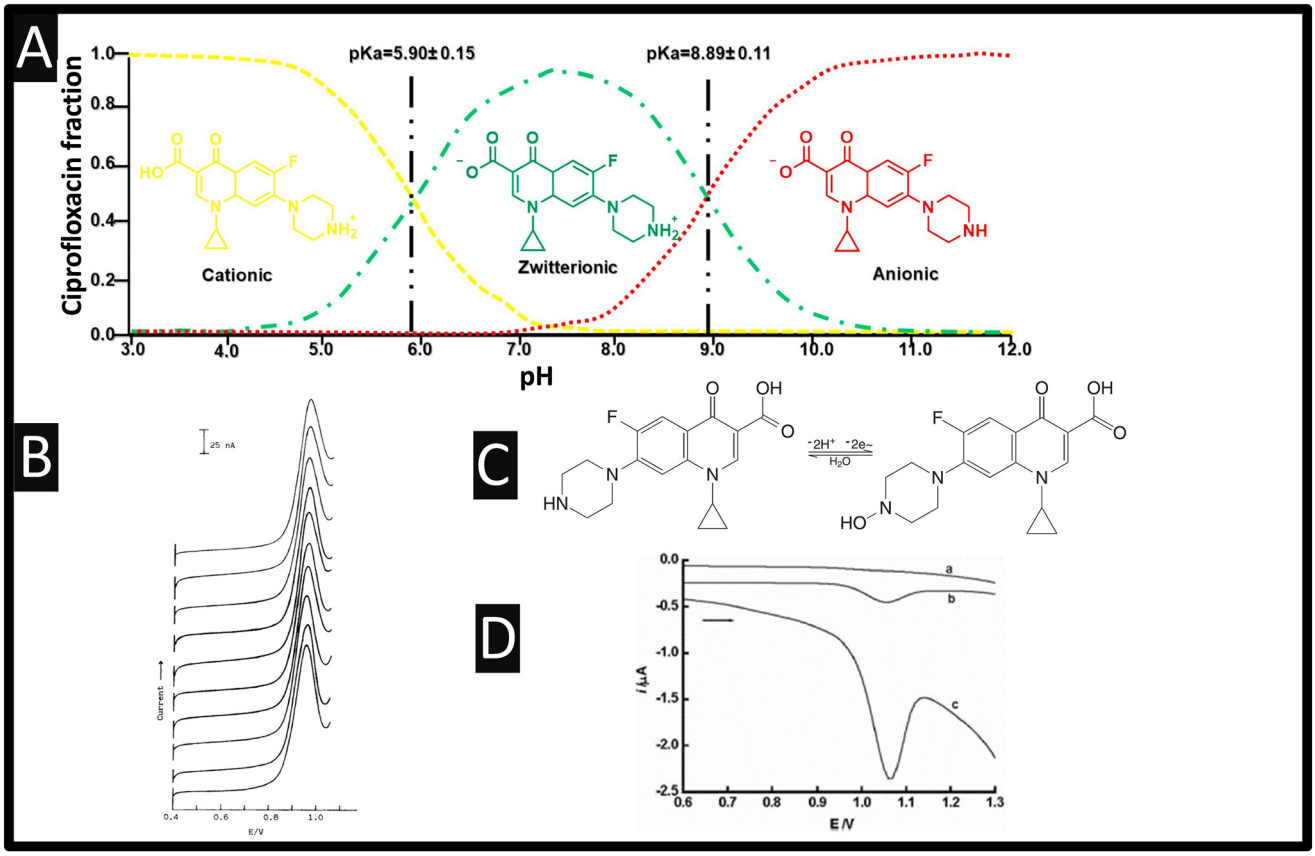

Fig. 1 A: Distribution molecular structure of ciprofloxacin as a function of pH; reproduced from ref. 2. Copyright 2018 Elsevier; B: Reproducibility of the linear sweep voltammetric signal. Ten successive voltammograms of 0.2 μM ciprofloxacin were recorded with high anodic potential activation of the electrode surface before each measurement. Reproduced from ref. 5. Copyright 1991 Wiley. C: The electrochemical mechanism of ciprofloxacin; D: DPV of ciprofloxacin at CPE in pH 4.0 buffer. (a): Blank voltammograms, (b): 0.2 μM ciprofloxacin, (c): (b) +100 μM SDBS. The DPV parameters: pulse amplitude: 50 mV, scan rate: 20 mV s^{-1}, pulse width: 50 ms, accumulation time: 2 min figure reproduced from ref. 6. Copyright 2007 Korean Chemical Society, Seoul & Wiley-VCH GmbH.

which are unable to remove the substance, thus active antibiotics are present within wastewater which can lead to antimicrobial resistance.[4] Ciprofloxacin is a concern from a public health perspective, where there are no environmental quality standards and no information regarding its maximum residual limit in water mentioned in the literatures and documents of drug regulators such as the World Health Organization,[3] but under Council Regulation EEC/2377/90, the maximum residual limit of ciprofloxacin in milk is 100 ppb (0.3018 μM), while within poultry meat it is 100 μg kg^{-1} respectively.[3,4]

Various approaches for the measurement of ciprofloxacin have been reported, including a high-performance liquid chromatographic (HPLC) method using fluorescence[7] and ultraviolet[8] detection, sensitized lanthanide luminescence,[9] and capillary electrophoresis,[10] but they generally require skilled personnel and costly instruments, limiting their practical application and development. Another approach is electrochemical based, where an electrode is modified with desired materials that can give rise to beneficial electroanalytical signal. This methodology is extremely popular due mainly to the small size of equipment, easy installation, low cost, simple sample preparation and the observed selectivity and sensitivity.[11] Furthermore, quantitative detection of ciprofloxacin can be performed using electroanalysis in a manner that is simpler and cost-effective than most available ciprofloxacin determination methods in clinical practice and for quality control in the

Craig E. Banks

Craig E. Banks holds a personal chair in chemistry and has published over 600 papers and works on next generation additive manufacturing electrochemical sensing platforms.

pharmaceutical industry. In this perspective, we overview the recent reports directed to the sensing of ciprofloxacin *via* electroanalytical approaches.

2. Electroanalytical based sensors for ciprofloxacin

Table 1 overviews the entire field in which, as we are writing, just under 100 papers have been directed toward the electroanalytical detection of ciprofloxacin. We can see that the first publication reporting the measurement of ciprofloxacin was reported with 1990 using mercury, which over the years, has progressed to reports utilising mediators, metal oxides, nanomaterials such as carbon nanotubes and graphene, and more recently, molecular imprinted polymers. All these have been reported as the basis of sensors that measure over the dynamic ranges of low micromolar and with nanomolar limits of detection (LOD). Herein we overview the journey of electroanalysts reporting on the most essential accounts for the sensing of ciprofloxacin.

The first electrochemical determination of ciprofloxacin was by O'Dea and co-workers[12] who studied its reduction with a static mercury drop electrode using differential pulse polarography and found a linear range from 0.5 to 30 μM with a limit of detection (LOD) found to be 0.2 μM. The authors demonstrated that this method could be used for the sensing of ciprofloxacin within pharmaceutical samples.[12] This work paved the way for ciprofloxacin to be determined by electroanalytical sensors. This work was then extended by the authors[12] who studied hanging mercury drop electrode (HMDE) and a carbon paste electrode (CPE) towards ciprofloxacin using adsorptive stripping voltammetry. They reported that the use of the HMDE is limited due to accumulation properties and rather the CPE was taken forward to the sensing within human urine, where interferents were removed by passing this through a C_{18} pack cartridge clean-up.[5] The authors found that by using CPEs *via* a high anodic potential, a reproducible electroanalytical signal could be achieved; please see Fig. 1B. Later, the sensing of ciprofloxacin at a HMDE reported using square-wave adsorptive voltammetry that they could measure from 25–250 μM with a LOD reported to be 7 nM.[13] The authors reported the approach could be utilised in spiked human urine by taking 0.5 mL and adding 1 mL of 5% $ZnSO_4$, 0.1 mL of NaOH and 1 mL of ethanol, observing recoveries between 106–110%. Of note, the authors also measured ciprofloxacin within a pharmaceutical tablet which was compared to UV-vis methodology which validated the electroanalytical sensor approach. The overall electrochemical oxidation mechanism is shown within Fig. 1C which undergoes 2 protons and 2 electrons.

2.1 Differential pulse and square-wave voltammetry

Zhang and Wei[6] observed the electrochemical response of a CPE which had been modified with sodium dodecyl benzene sulfonate (SDBS) using differential pulse voltammetry (DPV). As shown within Fig. 1D, the electrochemical oxidation of ciprofloxacin exhibits a weak oxidation peak which increases in the presence of SDBS; it is suggested that SDBS adsorbs onto the CPE surface *via* hydrophobic interaction between the C–H chain and graphite, altering the structure and properties at the CPE–solution interface.[6] A linear range of 0.08–5 μM with a low LOD of 0.02 μM was reported. The authors studied a range of interferences upon the sensing of 0.5 μM ciprofloxacin where a 500-fold concentration of uric acid, ascorbic acid, caffeine, dopamine, xanthine, vitamin E, and the 100-fold concentration of pefloxacin, ofloxacin, norfloxacin, trovafloxacin, and gatifloxacin, show minimal interference. Furthermore, of note, the authors examined the sensing of ciprofloxacin within eye drops and a tablet which was compared directly with HPLC, giving excellent agreement between the two methods. A similar approach was employed *via* SDBS except the surfactant was changed to cetyltrimethyl ammonium bromide (CTAB), which exhibited similar electroanalytical performances.[14] Furthermore, others have utilised CTAB with the use of mesoporous carbon which displays a linear range from 5 nM–20 μM, with a LOD reported to be very low at 1.5 nM, where the response was ascribed to two factors: (1) CTAB facilitates electron transfer of ciprofloxacin; and (2) the high surface area of mesoporous carbon, which accumulates adsorptive ciprofloxacin on the mesoporous carbon ciprofloxacin electrode surface.[15]

Multi-walled carbon nanotubes (MWCNTs) have been explored as the basis of ciprofloxacin detection[16–19] as they are reported to offer good electrical conductivity, high surface area, significant mechanical strength and good chemical stability.[20] They have also been known to promote electron transfer reactions when used as electrode modifying materials.[21,22] For instance, Ensafi and co-workers[16] report the use of a MWCNT modified glassy carbon electrode (GCE) sensor for the determination of enrofloxacin and ciprofloxacin since it is reported that enrofloxacin is de-ethylated to its primary metabolite, ciprofloxacin where both will be found in the bile and urine of animals receiving treatment. That said, the authors were able to measure both ciprofloxacin and enrofloxacin within spiked human urine, plasma and pharmaceutical samples.[16] Other work has explored the sensing of ciprofloxacin by MWCNTs dispersed in a porous Nafion® film on to a boron-doped diamond (BDD) electrode substrate. As shown within Fig. 2A, the most prominent peak is observed in the case of the porous Nafion®–MWCNT/BDD which is superior to a bare BDD, Nafion®/BDD, porous Nafion®/BDD and Nafion®–MWCNT/BDD.

This porous-Nafion–MWCNT/BDD electrode enhanced detection of ciprofloxacin due to selective adsorption, which was accomplished by a combination of electrostatic attraction at $-SO_3^-$ sites in the porous Nafion® film and the formation of charge assisted hydrogen bonding between ciprofloxacin and –COOH MWCNT surface functional groups, noting that

Table 1 An overview of the accomplishments directed to the electroanalytical sensing of ciprofloxacin

Electrode material	Electrode modification	Electroanalytical technique	Dynamic range	Limit of detection	Real sample composition	Ref.
Static mercury drop electrode	—	DPP	0.5–30 μM	0.2 μM	Pharmaceutical	12
HMDE; CPE	—	AdSV	0.6–4 μM	0.6 μM	Human urine	5
HMDE	—	SW-AdSV	25–250 μM	7 nM	Human urine and pharmaceutical	13
GCE	—	Rotating biosensor	0.02–65 μM	0.4 nM	Pharmaceutical	56
CPE	SDBS	DPV	0.08–5 μM	0.02 μM	Pharmaceutical	6
CPE	CTAB	DPV	0.1–20 μM	0.05 μM	Pharmaceutical	14
CPE	CTAB–mesoporous carbon	Ad-ASV	5 nM–20 μM	1.5 nM	Human serum and pharmaceutical	15
GCE	Poly(pyrrole-*N*-hydroxysuccinimide)/antibody	EIS	1×10^{-12}–1×10^{-6} g mL^{-1}	3 pM	NA	44
GCE	MWCNT	Amperometry	40–1000 μM	6 μM	Human serum and urine	17
GCE	MWCNT	LSV	3–1200 μM	0.9 μM	Human urine, plasma and pharmaceutical	16
BDDE	Porous-Nafion®–MWCNT	DPV	0.005–0.05, 0.05–10 μM	0.005 μM	Natural waters and wastewater effluents	18
GCE	COOH-functionalized MWCNT	SWV	5–100 μM	0.16 μM	Hospital effluent and wastewater	19
SPE	Nanocellulose and polypyrrole/SWCNT	SWV	1–50 μM	0.196 nM	Human serum, lake water and pharmaceutical	23
SPCE	CNT–V_2O_5–chitosan	EIS	0.5–64.0 ng mL^{-1}	0.5 ng mL^{-1}	Milk	45
GCE	$MgFe_2O_4$–MWCNTs	CV	0.10–1000 μM	10 nM	Human plasma and urine	46
GCE	$CoFe_2O_4$–MWCNT	DPV	0.1–20 μM	0.036 μM	NA	47
GCE	$ZnWO_4$/carbon black	DPV	0.02–120 μM	0.02 μM	River and tap water	57
CPE	Chitosan coated Fe_3O_4 magnetic nanoparticles	DPV	0.05–75 μM	0.01 μM	Human serum and urine	58
CPE	Poly(L-tyrosine)/SnO_2 nanoparticles	DPV	10–100 μM	6.4 μM	Tablets	59
GCE	Nano-SnO_2/PVS	DPV	0.012–5 μM	6 nM	NA	60
GCE	Ru–Cu–TMA	DPV	2.5–100 μM	3.29 nM	Tap and sea water	61
GCE	NH_2-UiO-66/rGO	ASV	0.02–1 μM	6.67 nM	Tap and lake water	55
CPE	Copper zinc ferrite	ASV	0.909 μM–4.70 mM	25.8 nM	Human serum and urine	62
CPE	Poly-β-cyclodextrin and L-arginine	DPV	0.0 5–100 μM	10 nM	Human serum and pharmaceutical	27
CPE	2-Amino-5-mercapto-1,3,4-thiadiazole/Ag nanocrystals	DPV	18–180 μM	5 nM	Human urine and eye drops	63
GCE	Fe_3O_4@Pt NPs	Electrochemiluminescence	2–3000 pM	0.598 pM	Meat samples	43
GCE	TiO_2/PVA	DPV	10–120 μM	0.04 μM	Rainwater	64
GCE	$Ba_{0.5}Co_{0.5}Fe_2O_4$ NPs	LSV	10 nM–0.5 mM	5.8 nM	Pharmaceutical	65
GCE	PEI@Fe_3O_4@CNTS	DPV	0.03–70 μM	0.003 μM	Human serum, urine, and pharmaceutical	66
GCE	NiO NPs-GO-chitosan: EPH	SWV	0.040–0.97 μM	6 nM	Human urine and serum	28
GCE	Thiol functionalized LAPONITE®	DPV	10–110 μM	0.2 μM	Pharmaceutical	67
CPE	Poly-murexide	DPV	0.05–3.0 μM	0.0057 μM	Human serum and pharmaceutical	68
GCE	$BaCuSi_4O_{10}$	DPV	0.05–150 μM	9 nM	Water and wastewater effluents	69
SPE	V_2O_5	DPV	0.04–365 μM	0.01 μM	Human urine and pharmaceutical	70
CPE	Co/TiO_2 nanocomposite	DPV	0.1–70 μM	0.03 μM	Human urine and serum	71

Table 1 *(continued)*

Electrode material	Electrode modification	Electroanalytical technique	Dynamic range	Limit of detection	Real sample composition	Ref.
GCE	rGO/poly(phenol red)	DPV	0.002–0.05 μM; 0.05–400 μM	0.002 μM	Animal serum	72
SPE	AuNPs/CHI	SWV	0.1–150 μM	0.001 μM	Human serum, plasma, urine	73
Graphite paste electrode	Sm_2O_3 nanorods	DPV	0.05–170 μM	5 nM	Urine and pharmaceutical samples	74
GCE	CdS QDs	DPV	0.1–10 μM	22 nM	Urine	75
GCE	AuNPs/activated carbon	DPV	0.5–25 nM	0.20 nM	Milk and pharmaceutical	30
CPE	Poly (Evans blue) sodium dodecyl sulphate	CV	2–45 μM	0.183 μM	Pharmaceutical	76
GCE	PANI–β-CD/MWCNT	CV	10–80 μM	50 nM	Wastewater	77
GCE	Nitrogen doped carbon	DPV	0.25–100 μM	8 nM	Ground and tap water	78
CPE	CdTe quantum dots	DPV	25 nM–12 μM	42 nM	Pharmaceutical	79
BDD		SWV	0.15–2.11 μM	0.05 μM	Human urine	80
GCE	Au NP–β-CD–rGO	DPV	0.01–120 μM	2.7 nM	Tap water	81
GCE	rGO	Flow injection analysis with amperometry	1–100 μM	0.1 μM	Pharmaceutical and milk	82
GCE	CQDs/ZnO-NFs/poly(CTAB)	DPV	0.01–30 μM	1.97 nM	Human serum, urine pharmaceutical	83
GCE	Cu BTC	DPV	1–20 μM	0.47 nM	Tap water	84
GCE	Carbon nano spheres	DPV	0.1–2.5 μM	0.15 μM	Pharmaceutical and tap water	85
GCE	Ag_2MoO_4	Amperometry	0.04–240 μM	0.03 μM	NA	86
CPE	SDS/graphene	DPV	0.3–100 μM	0.029 μM	Human urine	87
Pt	PPy/Bi_2MoO_6/chitosan nanocomposites	DPV	0.01–1500 μM	40 μM	NA	88
ITO	BSA/anti-CPX/APTES/La_2O_3 NPs	DPV	0.001–0.5; 1–1000 ng L^{-1}	0.001 ng L^{-1}	Milk	89
BiFE	*Ceriodaphnia dubia*	SWV	8–200 ng L^{-1}	3 ng L^{-1}	NA	90
SPE	Oxygen-terminated BDDP	LSV	1–30 μM	0.588 μM	Artificial urine	91
Graphite electrode	TiO_2/PB/AuNPs/CMK-3/Nafion	CV	1–10 μM	0.108 μM	Wastewater	92
SPE	AuNPs/chitosan	SWV	0.1–150 μM	0.001 μM	Human serum, plasma and urine	73
CPE	Choline chloride	SWV	0.05–200 μM	36 nM	CIP eye drops, eggs, river water	93
GCE	Co–Fe-Prussian blue@CN	Amperometry	0.005–300; 325–741 μM	0.7389 nM	Human urine and bloodserum	94
GCE	Cuttlefish bone derived hydroxyapatite	SWV	0.01–1310 μM	91.8 nM	Human serum and urine	29
CPE	MWCNTs@MIP	DPV	0.005–0.85 μM	0.0017 μM	Human urine, serum, pharmaceutical	37
GCE	Chitosan/AuMIP	DPV	1–100 μM	210 nM	Mineral and tap water, milk and pharmaceutical	38
GCE	rGO/MIP	DPV	0.001–10 μM	0.09 μM	Pharmaceutical	39
GCE	rGO/MIP	DPV	0.001–0.5 μM	0.05 nM	Tap and pond water	40
SPE	Fe_3O_4 mag@MIP-CB-Nafion®	DPV	0.5–7.0 μM	8.4 nM	Synthetic urine, river water	41
CPE	Ag@POM@rGO–IL	SWV	0.103–122.88 μM	0.031 μM	Human serum and pharmaceutical	42
CPE	Graphene/Fe_3O_4 NPs	DPV	0.01–20 μM	1.8 nM	Tap and river water and antibiotic plant effluent	31
GCE	Cd^{2+}/graphene	ASV	0.1–10 μM	0.059 μM	Human urine and pharmaceutical	53
CPE	Nitrogen doped carbon porous reduced graphene oxide	DPV	0.1–10 μM	39 nM	Human blood serum, eye drop and pharmaceutical	32

Table 1 *(continued)*

Electrode material	Electrode modification	Electroanalytical technique	Dynamic range	Limit of detection	Real sample composition	Ref.
GCE	Au NPs/carbon nitride/graphene	SWV	0.6–120 μM	0.42 μM	Milk samples	33
GCE	Chemically-reduced graphene-oxide	SWV	6–40 μM	0.21 μM	Pharmaceutical and milk	95
GCE	Graphene	DPV	0.5–200 μM	0.02 μM	Pharmaceutical	96
SPE	Graphene	SWV	0.1–100 μM	0.1 μM	Human urine, serum	97
GCE	Graphene-sodium polyacrylate-Pd	DPV	0.18–10.8 μM, 10.8–180 μM	0.045 μM	Shrimp and sea cucumber	98
GCE	Poly(alizarin red)/electrodeposited graphene	DPV	0.08–120 μM	0.01 μM	Tablets and human serum	99
Potentiometric sensors	CPX-PM-NiO/CaO nanocomposite	—	0.1 nM–10 mM	63 μM	Pharmaceutical	48
Potentiometric sensors	MWCNTs-CPX-PM	—	10 mM–10 μM	7.9 μM	Human urine, serum and pharmaceutical	50
Potentiometric sensors	4-Quinolones–dioctylphthalate	—	10 mM–100 μM	50 μM	Pharmaceutical	52
Potentiometric sensors	Poly 2-(hydroxymethyl)thiophene	—	0.1–200 μM	7 nM	Human urine	51
SPE	GO	DPV	1.0–8.0 μM	0.30 μM	Milk	54
SPE	Oxygenated-BDD powder	LSV	10–3000 μM	0.588 μM	Artificial urine	91
SPE	AuNPs/chitosan polymer	SWV	0.1–150 μM	0.001 μM	Human serum, plasma and urine	73
Pencil graphite electrode	Iron-decorated graphitic carbon nitride	DPV	0.001–1.0 μM	5.4 nM	Human blood serum	100
BDD		DPV	0.5–60 μM	0.440 μM	Human urine	101
BDD		DPV	0.74–20.0 μM	0.6 μM	Human urine	102
GCE	CdO/PANI/mpg-C_3N_4	DPV	0.01–20; 25–250 μM	5 nM	Human blood serum	34
Pencil graphite		SWV	12–55 μM	5.6 μM	Pharmaceutical	57
Pencil graphite	MIP	SWV	1 nM–1 mM	75 pM	Pharmaceutical	103
Paper based electrode		DPV	9.90–220 μM	4.96 μM	Milk and honey	35
Exfoliated pencil graphite electrode		SWV	5–100 μM	0.35 μM	Milk, water and pharmaceutical	104

Key: DPP: differential pulse polarography; CV: cyclic voltammetry; AdSV: adsorptive stripping voltammetry; SWV: square-wave voltammetry; SW-AdSV: square-wave adsorptive stripping voltammetry; SDBS: sodium dodecyl benzene sulfonate; MWCNTs: multi-walled carbon nanotubes; EIS: electrochemical impedance spectroscopy; Ad-ASV: adsorptive anodic stripping voltammetry; LSV: linear sweep voltammetry; CNT: carbon nanotubes; DPV: differential pulse voltammetry; rGO: reduced graphene oxide; PVA: poly(vinyl alcohol); EPH: epichlorohydrin; AuNPs: gold nanoparticles; β-CD: β-cyclodextrin; ZnO-NFs: zinc oxides nanoflowers; SDS: sodium dodecyl sulfate; BSA: bovine serum albumin; APTES: (3-aminopropyl)trimethoxysilane; BDDP: boron-doped diamond powder; SPE: screen-printed carbon electrode; BDD: boron-doped diamond; MIP: molecularly imprinted polymers; CB: carbon black; MIP: molecularly imprinted polymer; mag@MIP: magnetic Fe_3O_4 nanoparticles coated with molecularly imprinted polymers; Ch-AuMIP: chitosan gold nanoparticles decorated molecularly imprinted polymers; PEI: polyethylenimine; HMDEs: hanging mercury drop electrodes; PVS: poly(vinyl sulfonic potassium); Ru-Cu-TMA: ruthenium doped copper–trimesic acid; CTAB: cetyltrimethyl ammonium bromide; CPX-PM: ciprofloxacin phosphomolybdate.

the bare BDD electrode did not show any activity for the electrochemical oxidation of ciprofloxacin (Fig. 2B). This sensor was shown to be linear over the range 0.005–0.05 μM and 0.05–10 μM with a LOD of 5 nM. This sensor was selective for ciprofloxacin detection in the presence of other antibiotics *i.e.*, amoxicillin and other nontarget water constituents: Cl^-, Ca^{2+}, humic acid, sodium dodecylbenzenesulfonate, salicylic acid, 4-aminobenzoic acid, and 4-hydroxybenzoic acid. However, the sensor suffered fouling at high concentrations of 1 mM 4-aminobenzoic acid and 4-hydroxybenzoic acid, nevertheless, a short cathodic treatment fully restored sensor response.[18] Other work has utilised carboxylated MWCNTs, which they applied to the measurement of ciprofloxacin within hospital effluent and wastewater with recoveries of 99.4–105.8%.[19] Related to MWCNTs are single-walled nanotubes (SWCNTs) which have been incorporated with nanocellulose (NNC) and polypyrrole (PPY), and deposited upon a screen-printed electrode (SPE) for the simultaneous determination of paracetamol and ciprofloxacin.[23] The benefits of SPEs can be found within the following ref. 24–26. The fabricated NNC–PPY/SWCNTs/SPE was shown to give rise to the largest electrochemical area which showed dynamic linear range of 0.05–40.0 μM and 1–50 μM for paracetamol and ciprofloxacin and a limit of detection (LOD) of 0.072 nM and 0.196 nM respectively; please see Fig. 2C for an overview. The authors applied their

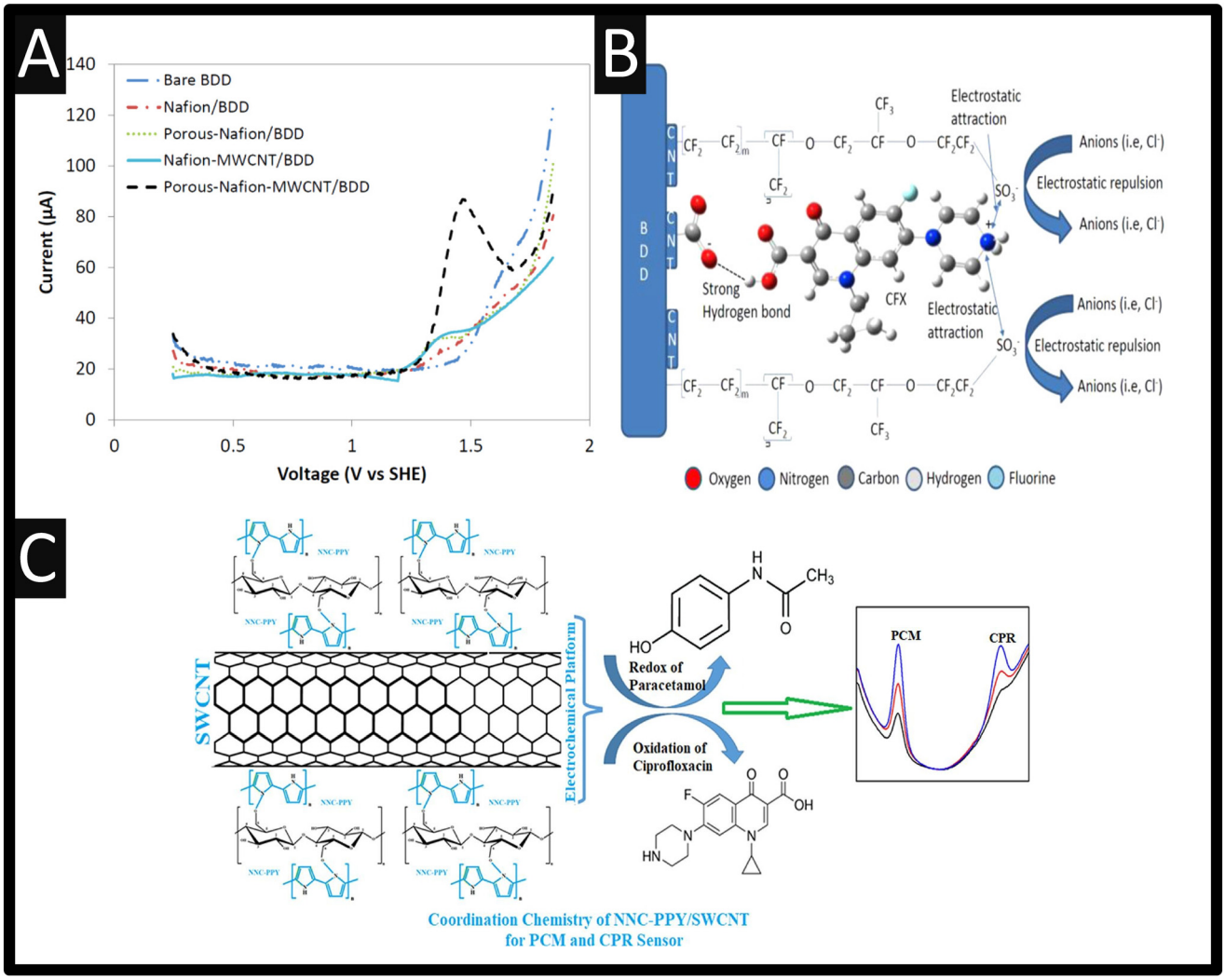

Fig. 2 A: Differential pulse voltammetry of 50 μM ciprofloxacin on BDD, Nafion®/BDD, porous-Nafion®/BDD, Nafion–MWCNT/BDD, and porous-Nafion®–MWCNT/BDD electrodes (pH = 4.50); B: A schematic overview of how the porous-Nafion®/BDD detected ciprofloxacin. Figures reproduced from ref. 18. Copyright 2006 American Chemical Society. C: An overview of a NNC–PPY/SWCNTs/SPE sensor for the simultaneous measurement of paracetamol and ciprofloxacin. Figure reproduced from ref. 23. Copyright 2022 Elsevier.

sensor to determining both paracetamol and ciprofloxacin within human serum, lake water and a pharmaceutical.[23]

Other reports have developed the polymerization of β-cyclodextrin (β-CD) and L-arginine (L-arg) to produce a modified carbon paste electrode (CPE) (P-β-CD–L-arg/CPE) for the first time.[27] As shown within Fig. 3A, the electrochemical polymerisation was performed by placing a CPE into a solution containing L-arg and β-CD where the potential was cycled between −2.0 to +2.5 V for 10 cycles at a 100 mV s^{-1}. Using optimized conditions, this sensor was utilized to determine the concentrations of ciprofloxacin, ofloxacin, norfloxacin and gatifloxacin with the dynamic ranges and LOD of 0.05–100 μM and 10 nM for ciprofloxacin, 0.1–100 μM and 40 nM for ofloxacin, 0.1–40 μM and 40 nM for norfloxacin and 0.06–100 μM and 20 nM for gatifloxacin, respectively. Fig. 3A presents the overall mechanism is shown where inner cavities of β-CD could restrain the analytes to form stable host–guest inclusion complexes, and the guanidyl group of L-arg could enable L-arg to form electrostatic interactions with negatively charged groups COO^- of ciprofloxacin and the single –NH– of piperazine ring was oxidized to be N–OH.[27] This method was successfully used to detect the concentrations of each drug in pharmaceutical formulations and spiked human serum sample with a recovery of 90–106% and the RSD was lower than 4%; this suggests that this sensor exhibited good reproducibility, long-term stability and fast current response.[27]

Other approaches have utilised metal oxides, for example, a simple and highly selective electrochemical method based upon graphene oxide and nickel oxide nanoparticles (diameter ~ 24 nm) was the basis of a sensor developed for the simultaneous determination of paracetamol and ciprofloxacin;[28] see Fig. 3B. Under optimised conditions, using square-wave voltammetry (SWV), the simultaneous determination of paracetamol and ciprofloxacin exhibit two resolved peaks and a dynamic range from 0.10 to 2.9 μM and

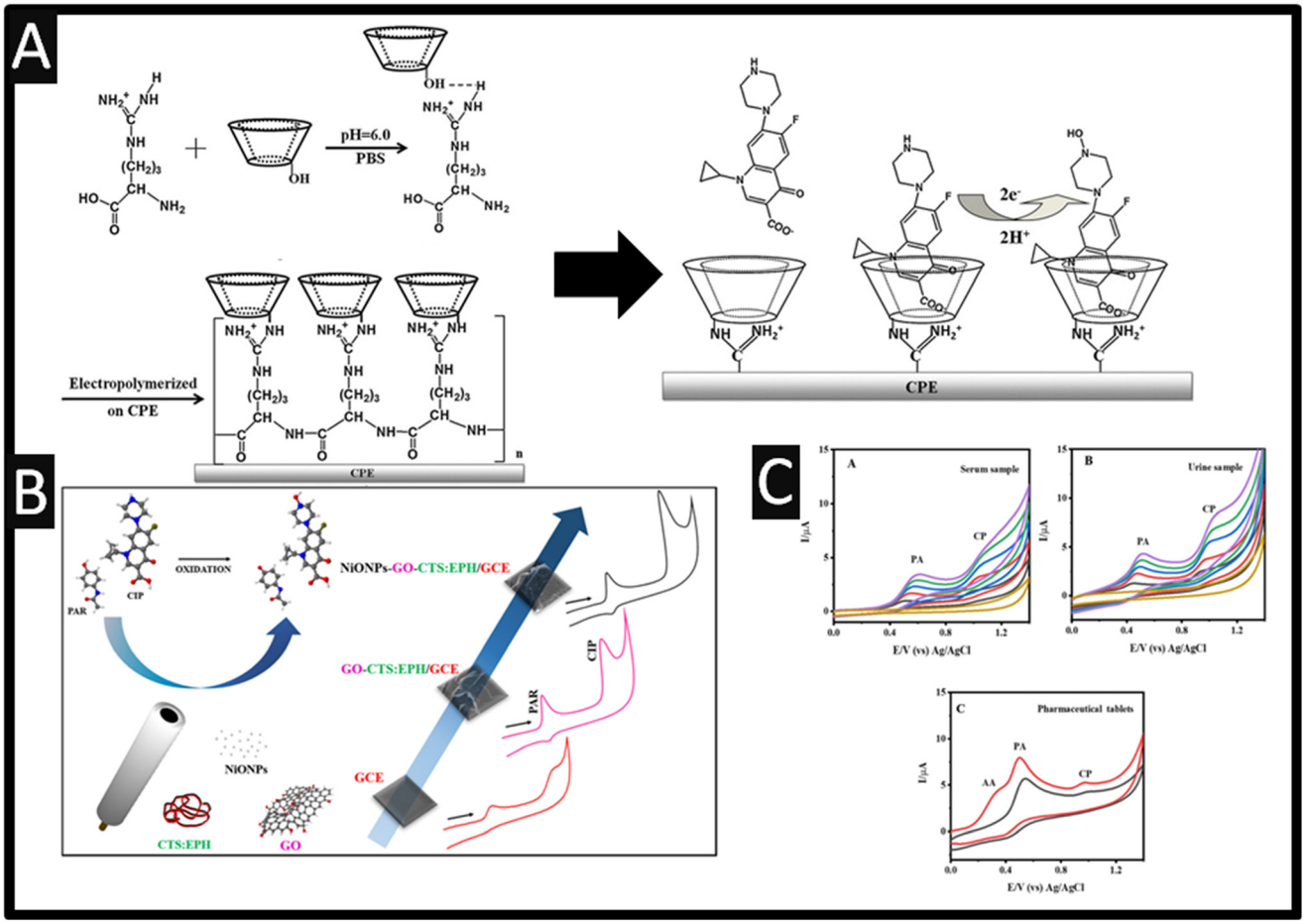

Fig. 3 A: Schematic representation of the probable electropolymerization process of β-CD and L-arg and the electrochemical reaction of ciprofloxacin on the P-β-CD–L-arg/CPE figures are reproduced from ref. 27. Copyright 2013 Elsevier. B: An overview of electrode fabrication and cyclic voltammetry showing the resolution between paracetamol and ciprofloxacin. Reproduced from ref. 28. Copyright 2017 Elsevier. C: CVs recorded at C-HAP in the presence of serum (A); and urine sample (B) followed by the standard addition of different concentration of PA and CP; (C) CVs recorded for the commercial pharmaceutical tablets at hydroxyapatite/GCE in 0.1 M PBS. Figure reproduced from ref. 29. Copyright 2023 Elsevier.

0.040 to 0.97 μM with LODs of 6.7 and 6.0 nM, respectively. The proposed sensor was successfully applied for the simultaneous determination of paracetamol and ciprofloxacin in synthetic spiked biological fluid samples. This work has been extended further, rather than measuring ciprofloxacin and paracetamol, Anitta and Sekar[29] developed a sensor for the measurement of ciprofloxacin, paracetamol in the presence of ascorbic acid, which utilised hydroxyapatite ($Ca_{10}(PO_4)_6(OH)_2$) synthesized by microwave irradiation method using cuttlefish bone-derived calcium source and synthetic diammonium phosphate; the average size of the hydroxyapatite was 300–400 nm. This sensor displayed a dynamic range 0.01–1310 μM and a LOD reported to be 91.8 nM. The practical use of the sensor was applied to the measurement of ciprofloxacin, paracetamol in the presence of ascorbic acid within human urine and serum, as shown within Fig. 3C. Note that these peaks are very close, closer than reported using nickel oxide with graphene oxide,[28] but sufficient to work. Through the use of activated carbon, which has been decorated with gold nanoparticles, a dynamic range of 0.5–25 nM with a LOD of 0.2 nM was achieved for the detection of ciprofloxacin.[30] Activated carbon was synthesized from used waste coffee grounds which were cleaned by KOH to remove interferences and dried in an oven for 2 h at 80 °C. The waste coffee ground precursor was then obtained and placed in a hydrothermal autoclave with KOH to produce the porous carbons. The activated carbon was dissolved in DMF which was drop cast upon a GCE. The activated carbon produced irregular shapes with a diameter of 2 μm. The gold nanoparticles were obtained by placing the activated carbon modified GCE into a gold salt solution which were electrochemically modified producing a particle size of 70 nm. Last, the electrode was modified by adding cationic SUPRAS. The authors studied the effect of interferences (20 nM) from other antibiotics such as amoxicillin (AMX), tetracycline (TC), oxytetracycline (OTC), enrofloxacin (ENR), ofloxacin (OFL) and norfloxacin (NOR) which only ENR, OFL, and NOR affected the electrochemical signal but the highest signal came from ciprofloxacin. Last, the sensor was validated within spiked raw, UHT and 0% fat

milk samples. The recovery of ciprofloxacin was achieved in the range of 78.6–110.2% with RSDs less than 8.4%. The authors propose that this method allows an easy and low-cost fabrication, while it is eco-friendly sensor from the usage of green solvent (SUPRAS) and the recycling of biomass waste (waste coffee ground) for the activated carbon precursor.

Graphene has also been utilised as the basis of sensors directed to the measurement of ciprofloxacin. For example, Zokhtareh and co-workers[31] have developed a bulk modified CPE with graphene nanosheets and Fe_3O_4 nanoparticles, as shown within Fig. 4A. Only the electrode was characterised by SEM, negating the use of Raman, which shows multi-layer graphene nanosheets. As shown within Fig. 4B(a–c), the authors proposed that the electrochemical detection was promoted by the negatively charged group on the surface of the graphene nanosheets reacting with the positively charged ciprofloxacin, facilitating the oxidation process.[31] Furthermore, a reaction occurs between hydroxyl groups on the surface of the iron oxide nanoparticles and the protonated N–H group on the ciprofloxacin.[31] The authors report that the sensor measures ciprofloxacin over the range 0.01–20 μM with a LOD reported to be low, at 1.8 nM (see Fig. 4C). Last, this sensor was evaluated within real samples for the measurement of ciprofloxacin within spiked tap, river and antibiotic plant effluent which reported recoveries arrange the range of 96.8–103%.

Reyhane *et al.*[32] have reported the use of nitrogen doped porous reduced graphene oxide, which gave a linear response of 0.1 to 10 μM with a LOD reported to be 39 nM. As shown within Fig. 5A, the presence of the nitrogen-doped reduced porous graphene oxide gives rise to a larger peak which was attributed to π–π stacking interaction formed between the large π conjugated structures of the nitrogen-doped reduced porous graphene oxide and ciprofloxacin.[32] Last, this method was shown to successfully detect ciprofloxacin within a pharmaceutical tablet, eye drop and human blood serum, and the approach was validated through comparison of UV-vis. Other work has reported the use of gold nanoparticles supported upon carbon nitride and graphene which reported a linear range of 0.6–120 μM with a LOD of 0.42 μM which was applied to spiked milk;[33] Fig. 5B shows how the authors made their composite electrode. Milk is a common analyte in which ciprofloxacin is measured – see Table 1. The authors took 10 mL of milk mixed with 5 mL of deionized water and 1 mL of ciprofloxacin (as the desired concentrations), which was incubated at room temperature for 24 h. After the

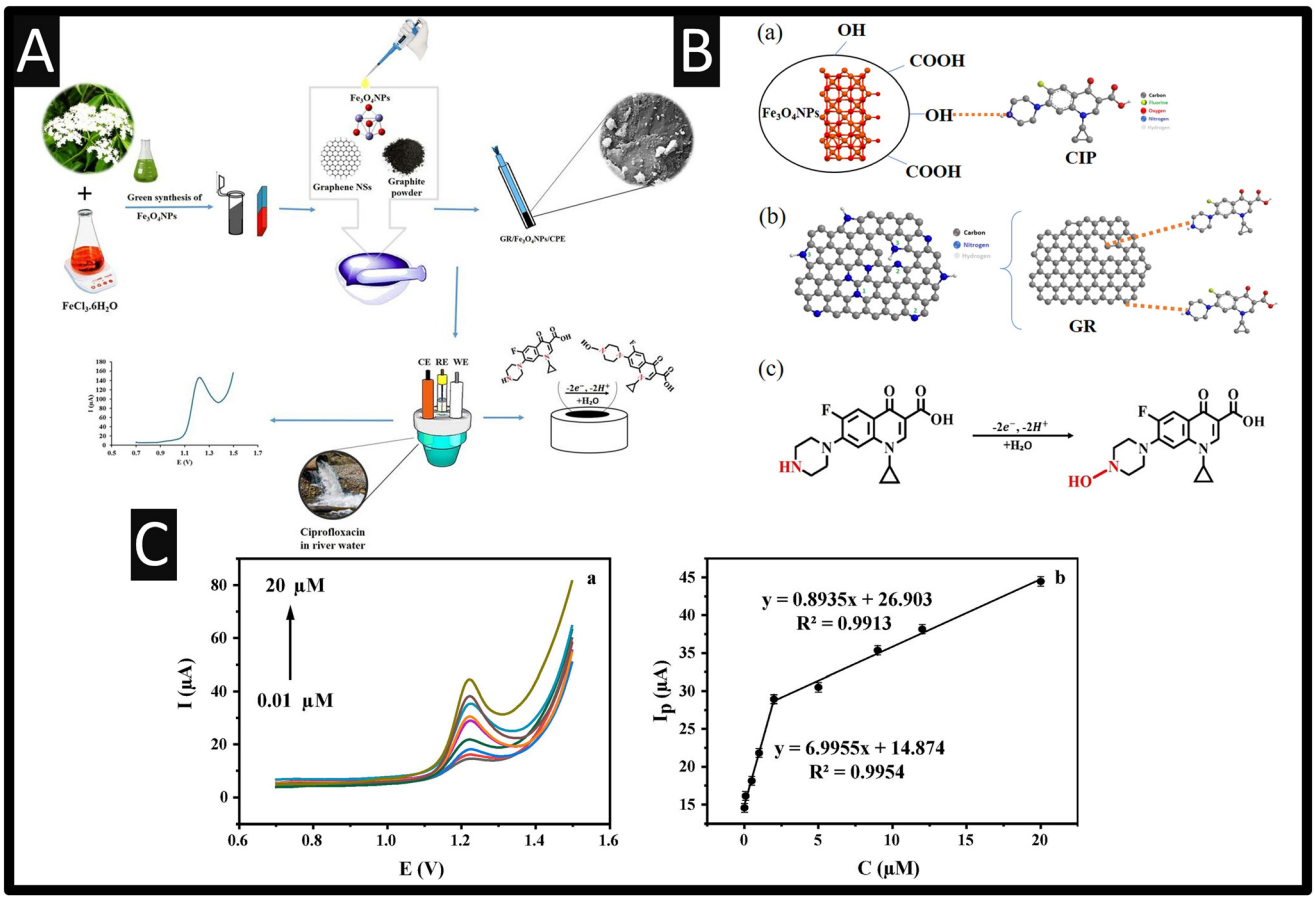

Fig. 4 A: An overview of how the authors constructed their sensor for ciprofloxacin. B: Possible mechanism of CIP oxidation at GR/Fe_3O_4NPs/CPE; C: DPVs of GR/Fe_3O_4NPs/CPE for diverse concentrations of CIP at GR/Fe_3O_4NPs/CPE (a) in 0.1 M PBS (pH 3)/0.1 M NaCl; scan rate: 50 mV s^{-1} and the ciprofloxacin calibration plot (b). Figures reproduced from ref. 31. Copyright 2023 Wiley.

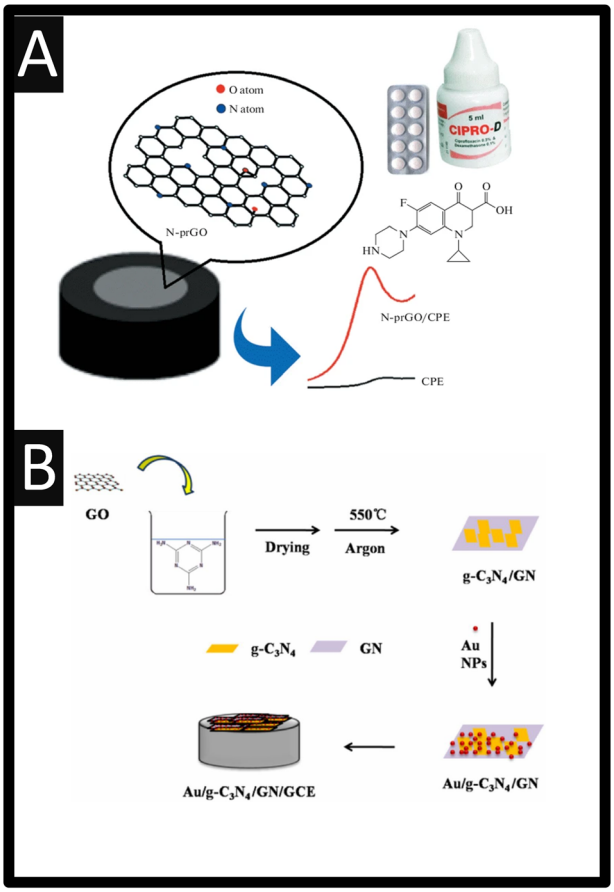

Fig. 5 A: Schematic illustration for the preparation of N-prGO/CPE to ciprofloxacin detection in pharmaceutical samples; figure reproduced from ref. 32. Copyright 2021 Springer. B: Schematic illustration of gold nanoparticles/carbon nitride/graphene modified glassy carbon electrode. Figure reproduced from ref. 33. Copyright 2018 The Electrochemical Society.

incubation was completed, 2 mL of trichloroacetic acid (20%, w/w) was added to the mixed system to precipitate proteins.[33] The authors demonstrated that the spiked milk with ciprofloxacin was possible with recoveries between 93.6–101.2%.

Carbon nitride (C_3N_4) is a fascinating class of N-doped carbon-based materials with a unique 2D structure which has high chemical and thermal stability, no risk to human health, environmental friendliness, and tuneable electronic structure.[34] Bonyadi and co-workers developed a sensor for the simultaneous determination of epinephrine, paracetamol, mefenamic acid and ciprofloxacin based upon a three-dimensional mesoporous polymeric graphitic-C_3N_4/polyaniline/CdO (mpg-C_3N_4/PANI/CdO) nanocomposite. Their approach is simple, which involved carbon nitride being synthesised *via* a one-step electrochemical method where platinum electrodes are placed into a solution of melamine applying a potential of +5 V for 60 min. Next, this was drop-cast onto a GCE and then electrochemically deposited with PANI *via* holding the potential at +1 V for 150 seconds. As depicted within Fig. 6Ai–iv, the electrochemical responses are shown. As can be seen, at the bare GCE electrode (Fig. 6Ai), epinephrine, paracetamol, mefenamic acid gives rise to voltammetric peaks but for ciprofloxacin none were seen. Using their sensor, as shown within Fig. 6Aii, epinephrine, paracetamol, mefenamic acid gives rise to voltammetric peaks but in the case of ciprofloxacin, the current has raised by two-fold. Next as show within Fig. 6Aiii, using GCE/mpg-C_3N_4/PANI surface, again the peaks shifted to negative values but as shown within Fig. 6Aiv, using a GCE/mpg-C_3N_4/PANI/CdO surface shows the best result which is attributed to the excellent electrocatalytic and conductivity of the mpg-C_3N_4/PANI/CdO nanocomposite.[34] Fig. 6B shows the voltammetric calibration plot for the simultaneous detection of epinephrine, paracetamol, mefenamic acid and ciprofloxacin, where in the case of ciprofloxacin a linear range of 0.01–20 and 25–250 μM with a LOD of 5 nM. The authors show that they can readily detect epinephrine, paracetamol, mefenamic acid and ciprofloxacin within human blood serum.

Related to SPEs is a report that uses a paper-based electrochemical sensor for the sensing of ciprofloxacin and exhibited a linear range from 9.90–220 μM with a LOD reported to be 4.96 μM.[35] This sensor was fabricated by taking graphite powder, which was mixed with nail polish diluted within acetone. This was homogenized and placed onto a paper substrate, which was dried in the oven to remove the solvent. Interestingly, the authors demonstrated their sensor could measure ciprofloxacin within spiked milk and honey by simply diluting the milk sample by 10-fold with water, while the honey was dissolved into water with the recoveries were 84–93%.[35]

Another tactic is the use of molecular imprinted polymers (MIPs), which are a synthetic recognition element that can be tailor-made to match an analytical target.[36] Research into the use of MIPs for the measurement of biosensors, and namely ciprofloxacin is expanding.[37–40] MIPs are supported with the use of magnetic multi-walled carbon nanotubes,[37] a chitosan gold nanoparticles decorated molecularly imprinted polymer,[38] through the use of reduced graphene oxide[39,40] and also magnetic Fe_3O_4 nanoparticles, which all exhibit nano to micromolar levels of ciprofloxacin sensing. As shown within Fig. 7A, an overview of how the authors fabricated their rGO/MIP.[40] The author utilised a glassy carbon electrode which was drop-casted with rGO, fabricated *via* a chemical exfoliation route.

Next the MIP was electrochemically polymerised with polyaniline–poly(*o*-phenylenediamine) in the presence of ciprofloxacin through potential cycling, after which, ciprofloxacin was eluted creating imprinted cavities on the MIP. This sensor was able to measure ciprofloxacin over the range of 0.001–0.5 μM with a LOD reported to be 0.00005 μM. Selectivity is key to MIPs and the authors examined

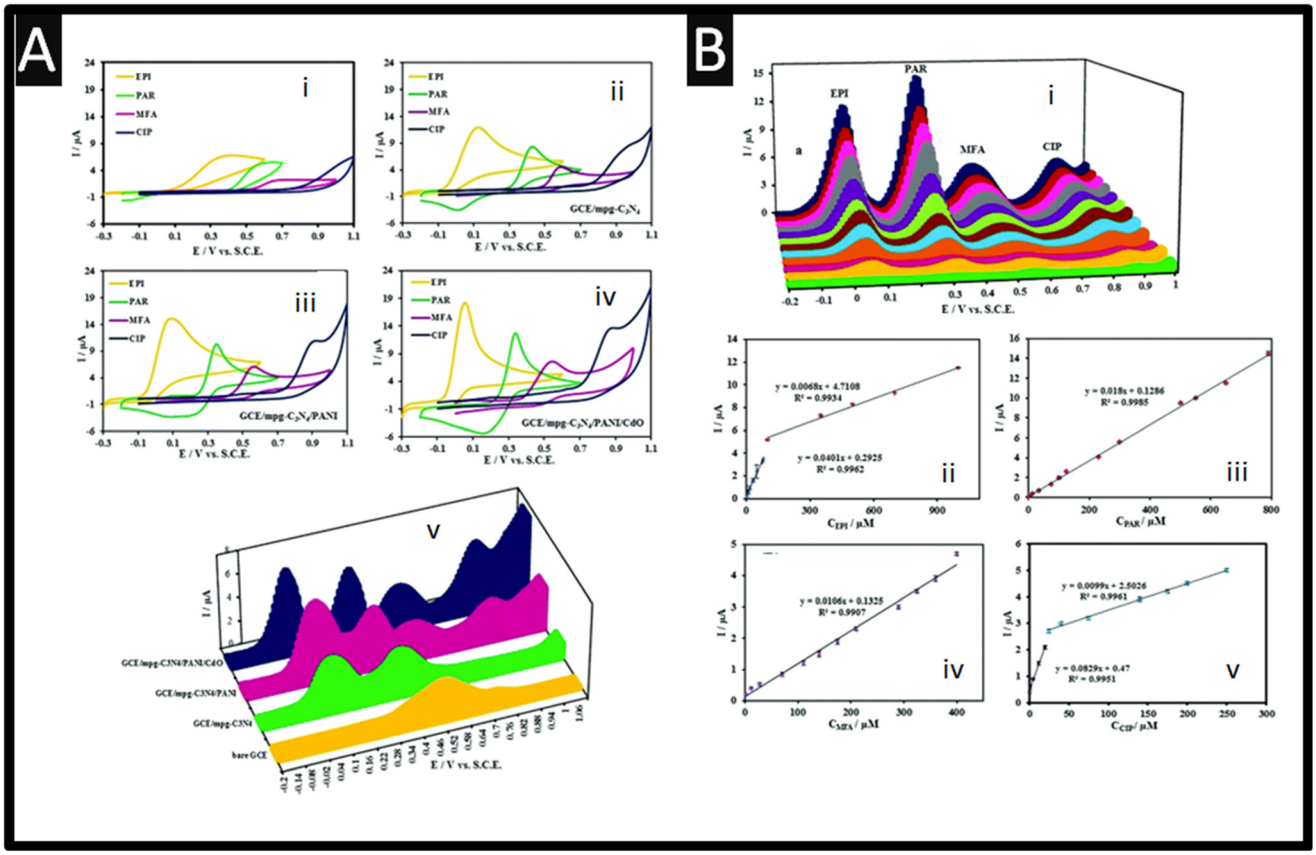

Fig. 6 A: Cyclic voltammograms of 500 μM EPI, PAR, MFA, and CIP at the bare GCE (i), GCE/mpg-C_3N_4 (ii), GCE/mpg-C_3N_4/PANI (iii), and GCE/mpg-C_3N_4/PANI/CdO (iv) in 0.1 M PBS (pH 7.4) at a scan rate of 100 mV s^{-1} and (v) differential pulse voltammograms of 250 μM EPI, PAR, MFA, and CIP at the bare GCE, GCE/mpg-C_3N_4, GCE/mpg-C_3N_4/PANI, and GCE/mpg-C_3N_4/PANI/CdO in 0.1 M PBS (pH 7.4). DPV experimental conditions: step: 0.005 V, modulation amplitude: 0.025 V, modulation time: 0.1 s, and interval time: 0.5 s. B: DPVs for different concentrations of EPI, PAR, MFA, and CIP mixtures. Current against concentration of EPI (ii), PAR (iii), MFA (iv) and CIP (v). DPV experimental conditions: step: 0.005 V, modulation amplitude: 0.025 V, modulation time: 0.1 s, and interval time: 0.5 s in 0.1 M PBS solution (pH 7.4). Figure reproduced from ref. 34. Copyright 2020 Royal Society of Chemistry.

antibiotic inferences enrofloxacin (ENR), ofloxacin (OFX), sulfamethoxazole (SMZ), and piperacillin sodium salt (PIP). The imprinting factor, α, is defined by: $\alpha = \frac{\Delta I(\text{MIP})}{\Delta(\text{NIP})}$, where the nonmolecular imprinted polymer (NIP) is fabricated the same as the MIP but without ciprofloxacin and also the selectivity factor, β, which is defined as: $\beta = \frac{\alpha(\text{ciprofloxacin})}{\alpha(\text{interferent})}$. The authors reported that α was for CIP, ENR, OFX, SMZ, and PIP are 1.7, 1.1, 1.0, 1.1, and 1.1, respectively, while for β, CIP, ENR, OFX, SMZ, and PIP are 1.0, 1.6, 1.6, 1.6, and 1.4, respectively, indicating that the sensor is more sensitive to CIP than other interference. The author demonstrated the use of their sensor through the sensing of ciprofloxacin within spiked tap and pond water.[40] Other notable work is the fabrication of SPEs modified with carbon black and magnetic Fe_3O_4 nanoparticles coated with a MIP.[41] In this approach, first the magnetic nanoparticles were prepared by a co-precipitation method which involves the use of iron(II) and iron(III) salts, which are placed into distilled water under stirring, where sodium hydroxide is added until the pH of 10 was obtained, resulting in magnetic iron nanoparticles in the range of 10–15 nm. Next, TEOS was added to the purified iron nanoparticles which was stirred for 12 h. The material (Fe_3O_4@SiO_2) was then added to MPS (methacryloxypropyltrimethoxysilane) and toluene producing Fe_3O_4@SiO_2–MPS nanoparticles. The mag@MIP was fabricated *via* photopolymerization where ciprofloxacin (template) it is dissolved with a functional monomer (methacrylic acid) into methanol, where Fe_3O_4@SiO_2–MPS nanoparticles which are stirred for 2 h. Next TRIM (a crossing reagent; trimethylolpropane trimethacrylate) and AIBN (a radical initiator, 2,2-azo-bisobutyronitrile) are added into the solution which was irradiated for 2 h which resulted in Fe_3O_4 mag@MIP. The sensor was fabricated by taking SPEs which were modified with carbon black (3–100 nm) and Nafion® upon which the Fe_3O_4 mag@MIP was drop casted. This sensor was used as outline within Fig. 7B, where process involving the capture and preconcentration of the analyte by Fe_3O_4 mag@MIP and

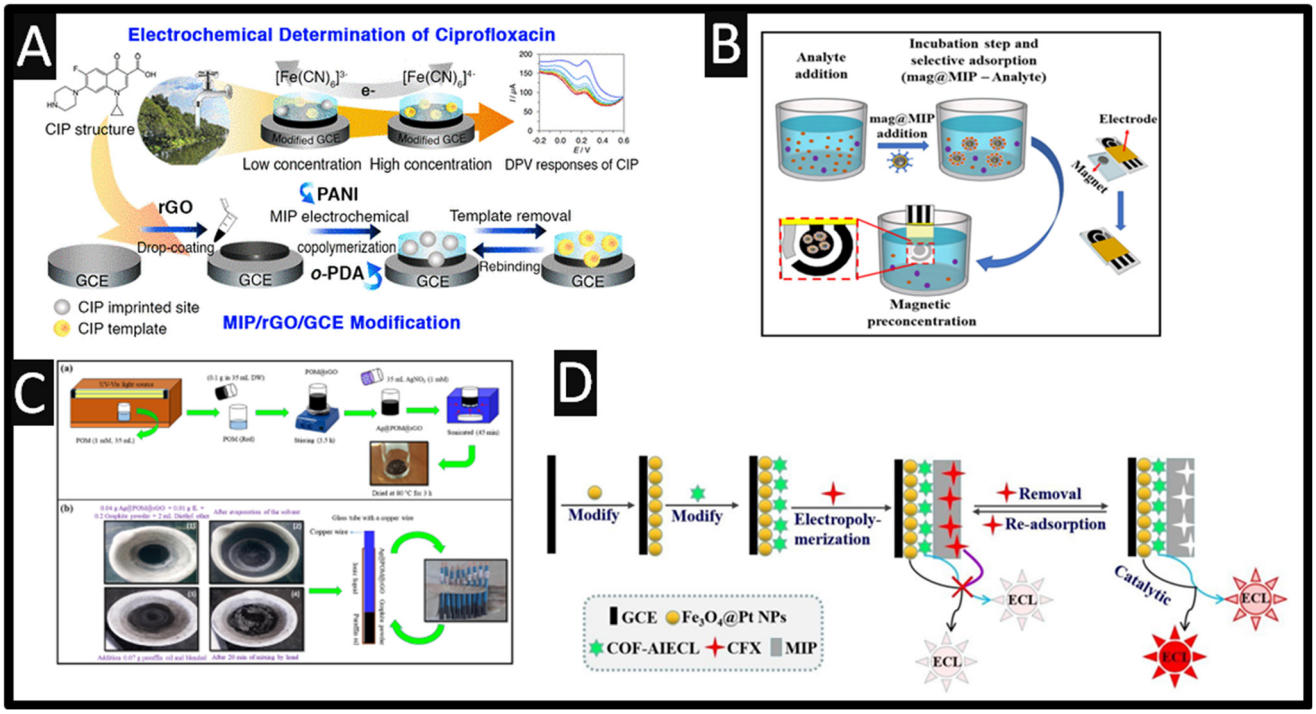

Fig. 7 A: An overview of how rGO/MIP sensing was achieved and their response towards ciprofloxacin. Reprinted with permission from ref. 40. Copyright 2023 American Chemical Society. B: Schematic representation of the selective adsorption and magnetic preconcentration of ciprofloxacin molecules promoted by the mag@MIP nanoparticles. The analyte/mag@MIP incubation process occurred in 1 min, under gentle agitation, using 1.0 mg of mag@MIP. Reproduced with permission from ref. 41. Copyright 2023 Wiley. C: Schematic illustration of the (a) steps for the synthesis of Ag@POM@rGO nanocomposite and (b) procedures for fabrication of the Ag@POM@rGO–IL/CPE. Reprinted with permission from ref. 42. Copyright 2023 Elsevier. D: Procedure for sensor fabrication for the detection of ciprofloxacin. Figure reproduced from ref. 43. Copyright 2022 Elsevier.

the subsequent electrooxidation of the analyte on the modified SPE surface. This sensor gave rise to a linear range of 0.5–7.0 μM with a low LOD reported to 8.4 nM; this sensor was shown to be successful in measuring ciprofloxacin within spiked urine and river water and was validated with HPLC where relative errors less than ±2.0% were observed. This work highlights the use of MIPs which provide selective synthetic recognition elements that has potential to be extended to other samples where ciprofloxacin needs to be determined. As shown within Fig. 7C, a CPE modified by silver decorated in polyoxometalate (POM), reduced graphene oxide (rGO) and ionic liquid (IL) was developed for measurement of ciprofloxacin (Ag@POM@rGO).[42] The advantages of CPE are reported as easy preparation, cheapness, renewability, uniform distribution of modifier into the paste, better reproducibility and stability, very low ohmic resistance and sufficient stability in aqueous solutions. In their protocol, POM, $H_3PW_{12}O_{40}$, was obtained from a commercial source, which it is reduced by exposure to a UV light source which was then mixed with rGO and stirred for 3.5 hours. Next, silver nitrate is added which it is sonicated for 45 minutes; the obtained powder was centrifuged, washed and then it was dried at 80 degrees for 3 hours. As shown within Fig. 7C, it is demonstrated how the Ag@POM@rGO–IL/CPE composite was prepared. The silver nanoparticles were conformed to be 4.5 nm in diameter which were homogeneously distributed upon the rGO surface. The authors demonstrated that this composite was able to measure ciprofloxacin over the range of 0.103–122.880 μM with a LOD reported to be 0.031 μM and was applied into spiked human plasma and pharmaceutical samples with good recoveries (99.84–102.33%). The authors noting that the procedure is easy, fast and inexpensive.[42]

Of note, from inspection of Table 1, the majority favour DPV and SWV which are both widely used electrochemical technique that offers several advantages over other electrochemical methods. These advantages make it a valuable tool for studying electrochemical reactions and analysing various types of samples. Some of the key advantages of DPV and SWV include: 1) high sensitivity, where both techniques are known for its high sensitivity, which allows for the detection of trace amounts of analytes in a sample where the techniques enhances the signal-to-noise ratio, making it easier to detect and quantify low concentrations of target compounds; 2) selectivity, both techniques can provide excellent selectivity by controlling the potential and analysing the resulting current response. By adjusting the potential scan range and parameters,

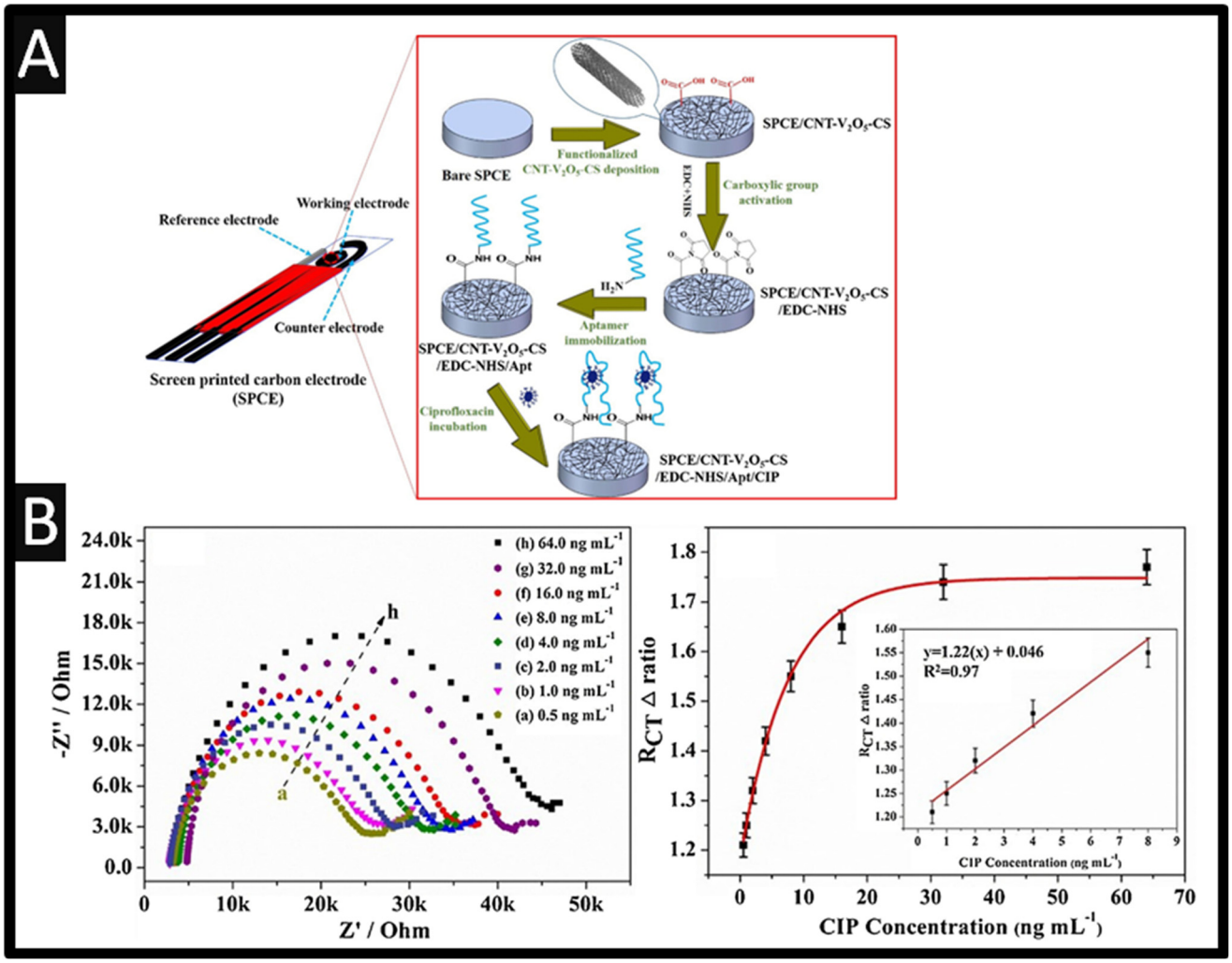

Fig. 8 A: Schematic representation of the electrode fabrication; B: Nyquist plots of SPCE/CNT–V_2O_5–CS/Apt electrode with different concentrations of CIP (ng mL^{-1}): (a) 0.5, (b) 1.0, (c) 2.0, (d) 4.0, (e) 8.0, (f) 16.0, (g) 32.0, (h) 64.0. The calibration curve of the ciprofloxacin aptamer corresponding to the detection of ciprofloxacin based on change in electron-transfer resistance (R_{ct}), which is presented as Δratio; the inset represents the linear region of the calibration curve of the aptasensor. Figures reproduced from ref. 45. Copyright 2018 Elsevier.

researchers can distinguish between different electroactive species in a complex mixture; 3) low background current, both techniques have a low background current, which means that it can be used to measure small changes in current accurately. This is particularly useful when dealing with samples containing interfering substances; 4) improved peak separation, where both techniques can resolve closely spaced peaks in the voltammogram more effectively than other techniques like cyclic voltammetry. This is especially important when studying complex mixtures of electroactive species; 5) quantitative analysis, both techniques are well-suited for quantitative analysis due to its ability to generate well-defined peaks and linear current–concentration relationships, making it easier to determine analyte concentrations accurately. Despite its many advantages, DPV and SWV also has limitations, such as the need for precise potential control and the potential for electrode fouling in some applications. The choice of electrochemical technique depends on the specific research objectives, but DPV and SWV remains a valuable tool for electrochemical analysis in many fields.

2.2 Electrochemiluminescence

A further sensitive method has been reported with a dynamic range of 2–3000 pM with a LOD of 0.598 pM using electrochemiluminescence and MIP based sensor with Fe_3O_4@Pt nanoparticle amplification for ultrasensitive ciprofloxacin detection.[43] As shown within Fig. 7D, the overview of how they fabricated their sensor. In their approach they made magnetic Fe_3O_4 nanoparticles, prepared *via* chemical co-precipitation with an average particle size of approximately 50 nm. Next, an organic framework with aggregation-induced ECL (COF-AIECL) was developed which involved a condensation reaction using [(1,3,5-triazine-2,4,6-triyl)tris(benzene-4,1-diyl)]triboronic acid and 1,2,4-

trimethylbenzene/1,6-dichlorohexane were added to the reactor and heated at 100 °C for 8 h. The sensor was obtained by drop-coating of Fe_3O_4@Pt NPs in *N*,*N*-dimethylformamide, which was dried using an infrared lamp. Then the COF-AIECL was immobilised with 1-ethyl-3-(3-dimethylaminopropyl)carbodiimide (EDC) and *N*-hydroxysuccinimide (NHS), which after 0.5 h, the COF-AIECL/Fe_3O_4@Pt NPs-modified GCE was obtained. This approach is due to the carboxyl in COF-AIECL being activated to form active ester by EDC and NHS, then the active ester reacted with the ammonia group on Fe_3O_4@Pt NPs to form amino bond. The mechanism is reported towards ciprofloxacin (CFX) as:

$$\text{COF-AIECL} - e^- \rightarrow \text{COF-AIECL}^{\bullet+}$$

$$H_2O_2 + e^- \rightarrow {}^{\bullet}OH + OH^-$$

$$H_2O_2 \rightarrow {}^{\bullet}OH + OH^-$$

$$\text{COF-AIECL}^{\bullet+} + OH^- \rightarrow \text{COF-AIECL}^*$$

$$\text{COF-AIECL}^* \rightarrow \text{COF-AIECL} + h\nu$$

$$\text{CFX} + e^- \rightarrow \text{CFX}^+$$

$$\text{CFX}^+ + \text{COF-AIECL}^* \rightarrow \text{COF-AIECL}^+ + \text{CFX}$$

The authors measured their methods into chicken, pork and beef meat samples, a total of 6 meat samples where only one, at a value of 0.102 nM pork had ciprofloxacin within; the authors compared the electroanalytical sensor against HPLC-MS which correlated well thus the developed sensor exhibited good reproducibility, stability, and selectivity for ciprofloxacin sensing in real applications.

2.3 Electrochemical impedance spectroscopy

One of the more sensitive measurements of ciprofloxacin has been reported by Giroud *et al.*[44] reporting an impedimetric immunosensor for the label-free detection of ciprofloxacin, where an electrochemically generated poly(pyrrole-*N*-hydroxysuccinimide) film was utilised. This sensor was able to report a LOD of 3 pM but unfortunately, there was no real sample utilised. Carbon nanotubes provide an excellent platform which they can support electrocatalysts. For instance, a novel aptasensing platform has been developed based on carbon nanotube (CNT)–V_2O_5–chitosan (CS) nanocomposites modified screen printed carbon electrode (SPEs) for the detection of ciprofloxacin.[45] The authors took commercially available MWCNTs and through the use of nitric acid, heated at 60 degrees for 24 h resulted in –COOH groups on the ends and sidewalls of the MWCNTs. These were then added with vanadium pentoxide at a ratio of 3 to 1 which was stirred overnight, then the precipitate was washed with acetone and then dried in an oven at 80 degrees. As shown within in Fig. 8A, a bare SPE was functionalised by CNT–V_2O_5 nanocomposites in a chitosan solution which were then coupled, through EDC and NHS, onto the surface in order to activate the terminal –COOH groups, after which the surface was modified by the aptamer. The authors utilised electrochemical impedance spectroscopy which was selected for the quantitative detection of ciprofloxacin and also reported that the aptasensor combines the biocompatibility of V_2O_5 nanoparticles, the efficient electron transfer capability of multiwalled CNTs, the effective film-forming strength of chitosan and the portability of SPEs.[45] As shown within Fig. 8B, the aptasensor exhibited a dynamic range from 0.5 to 64.0 ng mL^{-1}, where the linearity was between 0.5 to 8.0 ng mL^{-1} and the LOD was 0.5 ng mL^{-1}. The author verified the aptasensor in spiked milk samples and the acceptable recovery percentage of 94.50–97.87% (% RSD = 4.38, n = 3).[45] Others have been reported such as $MgFe_2O_4$–MWCNTs,[46] where the authors modified a GCE using an *in situ* citrate approach. This gave a dynamic range of 0.1–1000 μM with a low LOD of 10 nM, where the author showed their sensor could measure ciprofloxacin within human plasma and urine which was collaborated against HPLC. Others have followed the trend, with the use of $CoFe_2O_4$–MWCNTs.[47]

2.4 Potentiometric sensors

Another useful approach is the use of potentiometric sensors.[48] However, the use of potentiometric sensors are limited since the electroanalytical signal is strictly related on temperature and also the membrane potential is affected by the adsorption of solution components which limits their use.[49] Furthermore, potentiometric sensors can only detect only free ions and require frequent calibration plus there are many errors in forming the membrane.[49] That said, there are some examples of potentiometric sensors, for example, nickel oxide and calcium oxide (CaO) nanoparticles has been used where ciprofloxacin was coupled with phosphomolybdic acid (PMA) to give ciprofloxacin phosphomolybdate (CPX-PM) as an electrically active compound in the existence of polyvinyl chloride and the fluidizing medium *o*-nitrophenyl octyl ether (*o*-NPOE). The sensor exhibits a large linear range 0.1 nM–10 mM with a LOD of 63 μM. This was shown to useful for the sensing of ciprofloxacin within a pharmaceutical sample.[48] Other approaches have used MWCNTs,[50] poly 2-(hydroxymethyl)thiophene,[51] and 4-quinolones–dioctylphthalate[52] which report large linear ranges with low LODs, all have been successful in the sensing of ciprofloxacin within real samples.

2.5 Anodic stripping voltammetry

Another approach using graphene is the indirect determination of ciprofloxacin, utilising the anodic stripping voltammetry of cadmium(II) ions.[53] In this approach, the authors found that during the anodic

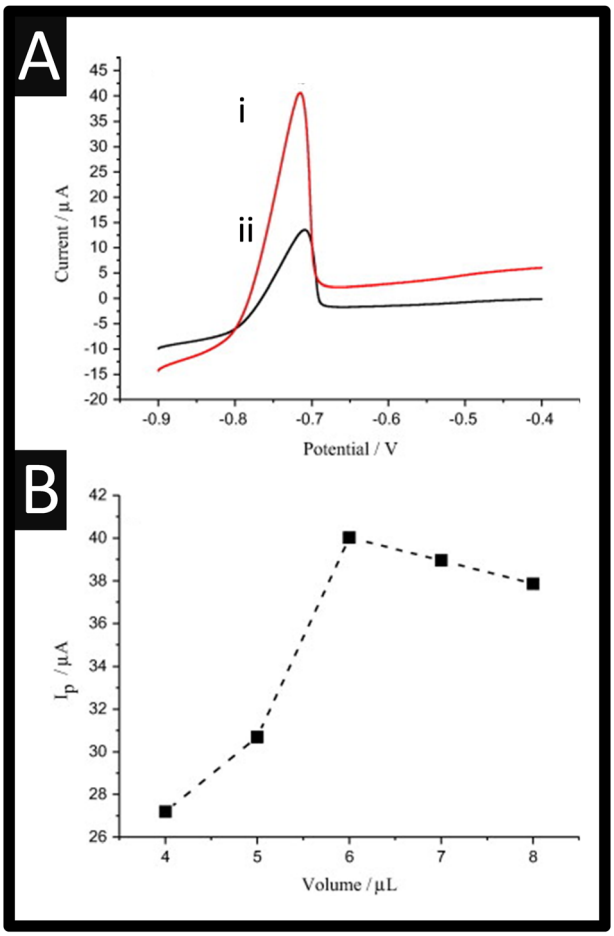

Fig. 9 A: Anodic stripping voltammetric curves of 1.0×10^{-4} mol L^{-1} Cd^{2+} in pH 3.6 at (i) bare GCE and (ii) graphene-modified GCE; B: influence of graphene amount on the peak current. Accumulation time: 10 s. Scan rate: 100 mV s^{-1}. Figure reproduced from ref. 53. Copyright 2015 Elsevier.

stripping voltammetry of cadmium(II) ions to cadmium metal in the presence of ciprofloxacin, the signal was magnified; see Fig. 9A for the enhancement and also the effect of graphene upon the peak current, Fig. 9B. Through this curious approach, it was able to show that the response occurred selectively towards ciprofloxacin over erythromycin, doxycycline, oxytetracycline and ofloxacin, which did not interfere. This approach allowed the authors to demonstrate their sensor was able to measure ciprofloxacin within spiked human urine and also a pharmaceutical, which was compared to HPLC which gave excellent results with a relative difference of 1.04%.[53] This work has been extended by replacing cadmium(II) ions with manganese(II) ions, which utilised a graphene oxide modified screen-printed electrode.[54]

Fang *et al.*[55] have reported the use of Zr(IV)-based metal–organic framework (MOF) NH_2-UiO-66 and rGO composites for the sensing of ciprofloxacin. In this approach, ciprofloxacin forms a stable composite with copper(II) ions due to a complexation reaction. They utilised the indirect measurement of Cu^{2+}, which decreases as the formations of the Cu^{2+}–ciprofloxacin occurs; see Fig. 10A. The sensor was fabricated through graphene oxide, which was prepared by the Hummers' method while the Zr-based MOF NH_2-UiO-66 was synthesized through a solvothermal method. In short, Zr(IV) was mixed with 2-aminoterephtalic acid and acetic acid which was ultrasonically treated for 30 min, after which, this mixture was autoclaved at 120 degrees for 16 h which formed NH_2-UiO-66. After cleaning with DMF, the mix was then heated at 80 degrees under vacuum overnight; see Fig. 10A. This NH_2-UiO-66 was coupled with rGO through dispersing within DMF and applying ultrasound for 2 h. TEM images of NH_2-UiO-66 is presented within Fig. 10B showing the particle size distributions and elemental mapping data. The anodic stripping voltammetry signatures are presented within Fig. 10C where the signal decreases as ciprofloxacin is added in due to the complexation reaction. This sensor was able to detect ciprofloxacin over the range of 0.02 to 1 μM where a LOD of 6.67 nM is reported. The sensor was validated though the measurement of ciprofloxacin within tap and lake water. The authors reported that the use of NH_2-UiO-66/rGO overcomes the MOFs low electrical conductivity.

Last, as summarised within Table 2, laboratory analytical protocols for the measurement of ciprofloxacin are compared with electrochemical determination methodology where it can be observed, that electrochemistry provides similar dynamic ranges which has been showed to be successful in real sample composition. Noting that laboratory techniques require, in some cases, a pre-analytical derivation step with liquid–liquid or solid phase extraction resulting in time-consuming procedures which can be simplified using electroanalytical approaches.

Conclusion and outlook

We have overviewed the use of electroanalysis as the basis of a sensor for the determination of ciprofloxacin exploring the lineage of electrodes utilised, from mercury to screen-printed electrodes. The electroanalytical sensing platforms produced used a wide-range of materials which reports useful dynamic ranges and low LODs and have been reported within useful matrices. Inspection of Table 1 shows that ciprofloxacin has been measured within human serum and urine while others try milk and meat samples; future work should extend the work on the latter samples and development other matrices. Most approaches explore real samples, but they only spike the solution being investigated where future work should compare directly with an independent laboratory techniques (such as HPLC) giving confidence that electrochemical sensors can be realised as an independent approach through commercialisation. A large proportion of these electrodes are considered through adaption of glassy carbon electrodes, with more recently adaptations performed to screen-printed

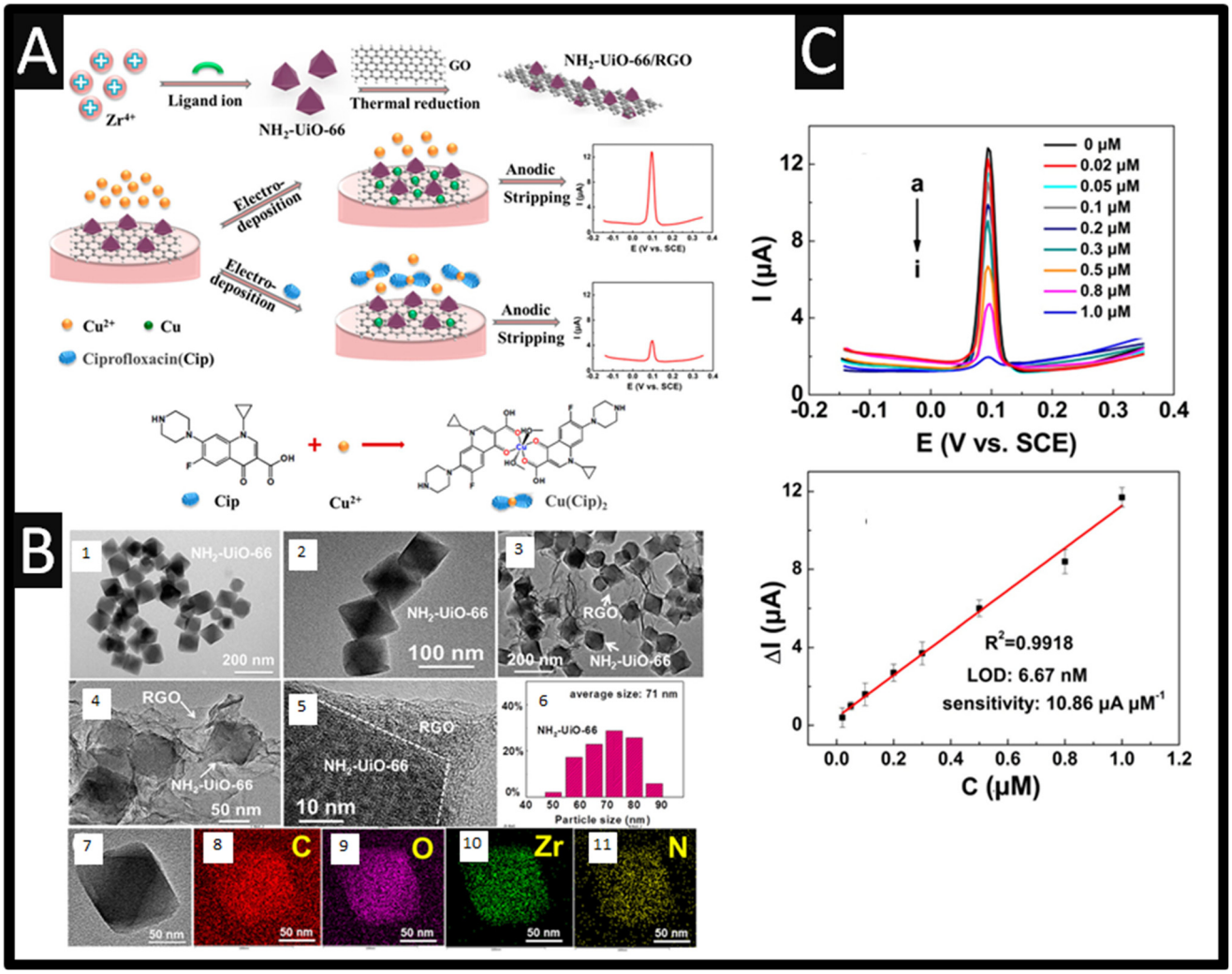

Fig. 10 A: Schematics of the NH_2-UiO-66/rGO synthesis procedure and the electrochemical detection of ciprofloxacin with the aid of Cu^{2+}; B: (1 and 2) TEM images of NH_2-UiO-66; (3 and 4) TEM images and (5) HRTEM image of NH_2-UiO-66/rGO. (6) Particle size distribution histogram of NH_2-UiO-66. TEM image (7) and the corresponding elemental mapping data (8–11) of NH_2-UiO-66; C: ASV responses of the sensor to different concentrations of ciprofloxacin (a–i: 0, 0.02, 0.05, 0.1, 0.2, 0.3, 0.5, 0.8, and 1.0 μM) in pH = 4 containing 0.5 μM Cu^{2+}. (B) The linear relationship between ΔI and the ciprofloxacin concentration. Error bars represent the standard deviation (n = 5). Figure reproduced from ref. 55. Copyright 2019 American Chemical Society.

Table 2 An overview of the analytical approaches for the sensing of ciprofloxacin

Determination methodology	Dynamic range	Limit of detection	Real sample composition	Ref.
Fluorescence	0.1–18 μM	0.0136 μM	Milk	105
HPLC-UV	0.51–130 μM	0.25 μM	Pharmaceuticals	106
Colorimetric	1–1000 μM	51 μM	Tap water and milk	107
LC-MS	75 nM–9 μM	75 nM	Human plasma	108
Electrochemical	1 nM–1 mM	75 pM	Pharmaceutical	103
Electrochemical	0.001–1.0 μM	5.4 nM	Human blood serum	100
Electrochemical	0.01–20 μM	1.8 nM	Tap and river water and antibiotic plant effluent	31

electrodes. We note that starting with a glassy carbon it is interested, but it will fail as industry will want high reproducible but yet economical sensors, and the only viable approach is the use of screen-printed electrodes. As the field of additively manufactured electrodes becomes more popular, we anticipate publications utilising these electrodes to be released which can bridge the gap between academia and industry since additively manufactured electrodes are highly reproducible and sensitive and easily scalable but yet are economic.

Author contributions

RDC: original draft, writing – review & editing. PSA: review & editing; CEB: conceptualization, methodology, resources, formal analysis, writing – original draft, validation, writing – review & editing.

Conflicts of interest

There are no conflicts to declare.

References

1 F. Van Bambeke, J. M. Michot, J. Van Eldere and P. M. Tulkens, *Clin. Microbiol. Infect.*, 2005, **11**, 256–280.
2 D. A. Palacio, B. L. Rivas and B. F. Urbano, *Chem. Eng. J.*, 2018, **351**, 85–93.
3 M. Girmatsion, H. Dong, B. Abraha, A. Mahmud, M. Kasimala, H. Gebremedhin, A. Adhanom, G. Lu, F. Yang and Y. Guo, *Anal. Chim. Acta*, 2022, **1221**, 340082.
4 A. Hayes, L. May Murray, I. Catherine Stanton, L. Zhang, J. Snape, W. Hugo Gaze and A. Kaye Murray, *Environ. Int.*, 2022, **169**, 107488.
5 P. O'Dea, A. C. Garcíc, A. J. M. Ordieres, P. T. Blanco and M. R. Smyth, *Electroanalysis*, 1991, **3**, 337–342.
6 S. Zhang and S. Wei, *Bull. Korean Chem. Soc.*, 2007, **28**, 543–546.
7 P. Teja-Isavadharm, D. Keeratithakul, G. Watt, H. K. Webster and M. D. Edstein, *Ther. Drug Monit.*, 1991, **13**, 263–267.
8 S. Zhai, M. R. Korrapati, X. Wei, S. Muppalla and R. E. Vestal, *J. Chromatogr. B: Biomed. Sci. Appl.*, 1995, **669**, 372–376.
9 S. Singha and K. H. Ahn, *Sensors*, 2016, **16**, 2065.
10 K. H. Bannefeld, H. Stass and G. Blaschke, *J. Chromatogr. B: Biomed. Sci. Appl.*, 1997, **692**, 453–459.
11 J. Wang, *Analytical Electrochemistry*, Wiley-VCH, 4th edn, 2023.
12 P. O'Dea, A. C. García, A. J. M. Ordieres, P. T. Blanco and M. R. Smyth, *Electroanalysis*, 1990, **2**, 637–641.
13 A. F. Al-Ghamdi and A. D. Bani-Yaseen, *Russ. J. Electrochem.*, 2014, **50**, 355–362.
14 H. Yi and C. Li, *Russ. J. Electrochem.*, 2007, **43**, 1377–1381.
15 M. Abdel-Galeil, M. Ghoneim, H. El-Desoky, T. Hattori and A. Matsuda, *J. Electrochem. Soc.*, 2015, **162**, H541.
16 A. A. Ensafi, M. Taei, T. Khayamian and F. Hasanpour, *Anal. Sci.*, 2010, **26**, 803–808.
17 L. Fotouhi and M. Alahyari, *Colloids Surf., B*, 2010, **81**, 110–114.
18 P. Gayen and B. P. Chaplin, *ACS Appl. Mater. Interfaces*, 2016, **8**, 1615–1626.
19 A. Chaabani, T. Ben Jabrallah and N. Belhadj Tahar, *Electrocatalysis*, 2022, **13**, 402–413.
20 R. D. Crapnell and C. E. Banks, *Microchim. Acta*, 2021, **188**, 1–23.
21 X. Ji, R. O. Kadara, J. Krussma, Q. Chen and C. E. Banks, *Electroanalysis*, 2010, **22**, 7–19.
22 C. Kalinke, R. D. Crapnell, E. Sigley, M. J. Whittingham, P. R. de Oliveira, L. C. Brazaca, B. C. Janegitz, J. A. Bonacin and C. E. Banks, *Chem. Eng. J.*, 2023, 143513.
23 M. Shalauddin, S. Akhter, W. Jeffrey Basirun, V. Sanghiran Lee and M. Rafie Johan, *Environ. Nanotechnol., Monit. Manage.*, 2022, **18**, 100691.
24 J. P. Metters, R. O. Kadara and C. E. Banks, *Analyst*, 2011, **136**, 1067–1076.
25 A. L. Squissato, R. A. A. Munoz, C. E. Banks and E. M. Richter, *ChemElectroChem*, 2020, **7**, 2211–2221.
26 A. García-Miranda Ferrari, S. J. Rowley-Neale and C. E. Banks, *Talanta Open*, 2021, **3**, 100032.
27 F. Zhang, S. Gu, Y. Ding, Z. Zhang and L. Li, *Anal. Chim. Acta*, 2013, **770**, 53–61.
28 A. Martin Santos, A. Wong, A. Araújo Almeida and O. Fatibello-Filho, *Talanta*, 2017, **174**, 610–618.
29 S. Anitta and C. Sekar, *Results Chem.*, 2023, **5**, 100816.
30 N. Gissawong, S. Srijaranai, S. Boonchiangma, P. Uppachai, K. Seehamart, S. Jantrasee, E. Moore and S. Mukdasai, *Microchim. Acta*, 2021, **188**, 208.
31 R. Zokhtareh, M. Rahimnejad, G. Najafpour-Darzi and H. Karimi-Maleh, *Measurement*, 2023, **215**, 112872.
32 R. Reyhane, B. Sabeti and F. Chekin, *Russ. J. Electrochem.*, 2021, **57**, 654–662.
33 Y. Yuan, F. Zhang, H. Wang, L. Gao and Z. Wang, *ECS J. Solid State Sci. Technol.*, 2018, **7**, M201.
34 S. Bonyadi, K. Ghanbari and M. Ghiasi, *New J. Chem.*, 2020, **44**, 3412–3424.
35 C. C. de Souza, G. F. Alves, T. P. Lisboa, M. A. C. Matos and R. C. Matos, *J. Food Compos. Anal.*, 2022, **112**, 104700.
36 R. D. Crapnell, N. C. Dempsey-Hibbert, M. Peeters, A. Tridente and C. E. Banks, *Talanta Open*, 2020, **2**, 100018.
37 H. Bagheri, H. Khoshsafar, S. Amidi and Y. Hosseinzadeh Ardakani, *Anal. Methods*, 2016, **8**, 3383–3390.
38 S. G. Surya, S. Khatoon, A. Ait Lahcen, A. T. H. Nguyen, B. B. Dzantiev, N. Tarannum and K. N. Salama, *RSC Adv.*, 2020, **10**, 12823–12832.
39 J. Chuiprasert, S. K. Boontanon, S. Srinives, N. Boontanon, C. Polprasert and N. Ramungul, *IOP Conf. Ser.: Earth Environ. Sci.*, 2022, **973**, 012003.
40 J. Chuiprasert, S. Srinives, N. Boontanon, C. Polprasert, N. Ramungul, N. Lertthanaphol, A. Karawek and S. K. Boontanon, *ACS Omega*, 2023, **8**, 2564–2574.
41 A. Wong, A. M. Santos, T. A. Silva, F. C. Moraes, O. Fatibello-Filho and M. D. P. T. Sotomayor, *Electroanalysis*, 2023, **35**, e202200165.
42 H. Shafiei and S. Karim Hassaninejad-Darzi, *J. Electroanal. Chem.*, 2023, **935**, 117321.
43 F. Beigmoradi, M. Rohani Moghadam, A. Bazmandegan-Shamili and H. R. Masoodi, *Microchem. J.*, 2022, **179**, 107633.
44 F. Giroud, K. Gorgy, C. Gondran, S. Cosnier, D. G. Pinacho, M. P. Marco and F. J. Sánchez-Baeza, *Anal. Chem.*, 2009, **81**, 8405–8409.
45 X. Hu, K. Y. Goud, V. S. Kumar, G. Catanante, Z. Li, Z. Zhu and J. L. Marty, *Sens. Actuators, B*, 2018, **268**, 278–286.

46 A. A. Ensafi, A. R. Allafchian and R. Mohammadzadeh, *Anal. Sci.*, 2012, **28**, 705–710.
47 A. Hosseini, E. Sohouli, M. Gholami, A. Sobhani-Nasab and S. A. Mirhosseini, *Anal. Bioanal. Electrochem.*, 2019, **11**, 996–1008.
48 R. A. Al-Sabbah, S. A. Al-Tamimi, N. A. Alarfaj and M. F. El-Tohamy, *Int. J. Electrochem. Sci.*, 2023, **18**, 100284.
49 M. S. Cosio, M. Scampicchio and S. Benedetti, in *Chemical Analysis of Food: Techniques and Applications*, ed. Y. Picó, Academic Press, Boston, 2012, pp. 219–247, DOI: **10.1016/B978-0-12-384862-8.00008-X**.
50 F. M. Abdel-Haleem, M. S. Rizk and I. H. A. Badr, *Electroanalysis*, 2017, **29**, 1172–1179.
51 M. Burç, Ö. Güngör and S. Titretir Duran, *Polym. Bull.*, 2023, DOI: **10.1007/s00289-023-04995-z**.
52 H. Avsec and S. Gomišček, *Anal. Chim. Acta*, 1992, **268**, 307–309.
53 J. Shan, Y. Liu, R. Li, C. Wu, L. Zhu and J. Zhang, *J. Electroanal. Chem.*, 2015, **738**, 123–129.
54 M. Pan, P. Guo, H. Liu, J. Lu and Q. Xie, *J. Anal. Sci. Technol.*, 2021, **12**, 55.
55 X. Fang, X. Chen, Y. Liu, Q. Li, Z. Zeng, T. Maiyalagan and S. Mao, *ACS Appl. Nano Mater.*, 2019, **2**, 2367–2376.
56 A. A. J. Torriero, J. J. J. Ruiz-Díaz, E. Salinas, E. J. Marchevsky, M. I. Sanz and J. Raba, *Talanta*, 2006, **69**, 691–699.
57 K. Mariappan, S. Alagarsamy, S.-M. Chen and S. Sakthinathan, *Materials*, 2023, **16**, 741.
58 S. Dehdashtian, M. B. Gholivand, M. Shamsipur, A. Azadbakht and Z. Karimi, *Can. J. Chem.*, 2016, **94**, 803–811.
59 M. P. Deepak and G. P. Mamatha, *Anal. Bioanal. Electrochem.*, 2015, **7**, 523–538.
60 Y. Cai, Y. Zhang, S. Su, S. Li and Y. Ni, *Front. Biosci.-Landmark*, 2007, **12**, 1946–1955.
61 M. V. Varsha and G. Nageswaran, *Microchem. J.*, 2023, **188**, 108481.
62 M. P. Kingsley, P. K. Kalambate and A. K. Srivastava, *RSC Adv.*, 2016, **6**, 15101–15111.
63 M. Tiwari, A. Kumar, U. Shankar and R. Prakash, *Biosens. Bioelectron.*, 2016, **85**, 529–535.
64 J. Zhao, P. Huang and W. Jin, *Int. J. Electrochem. Sci.*, 2021, **16**, 211018.
65 N. S. Osman, N. Thapliyal, W. S. Alwan, R. Karpoormath and T. Moyo, *J. Mater. Sci.: Mater. Electron.*, 2015, **26**, 5097–5105.
66 N. R. Jalal, T. Madrakian, A. Afkhami and M. Ghamsari, *J. Electroanal. Chem.*, 2019, **833**, 281–289.
67 K. Y. Tajeu, D. V. T. Ebunang, R. C. T. Tonleu, S. L. Z. Jiokeng, E. Ymele and I. K. Tonle, *J. Appl. Electrochem.*, 2021, **51**, 435–446.
68 M. K. Maala, N. Z. Abd EL-Atiy, A. E.-S. Mohamed and M. N. Rashed, *J. Environ. Stud.*, 2023, **3**, 401–417.
69 G. Muungani, V. Moodley and W. E. van Zyl, *J. Appl. Electrochem.*, 2022, **52**, 285–297.
70 S. Tajik, H. Beitollahi, R. Zaeimbashi, M. Sheikhshoaei, M. B. Askari and P. Salarizadeh, *J. Mater. Sci.: Mater. Electron.*, 2021, **32**, 17558–17567.
71 M. Shamsipur, M. B. Gholivand, S. Dehdashtian, M. Feyzi and F. Jafari, *Adv. Mater. Res.*, 2014, **829**, 563–567.
72 R. Chauhan, A. A. S. Gill, Z. Nate and R. Karpoormath, *J. Electroanal. Chem.*, 2020, **871**, 114254.
73 K. R. Reddy, P. K. Brahman and L. Suresh, *Measurement*, 2018, **127**, 175–186.
74 S. Biswas, H. Naskar, S. Pradhan, Y. Chen, Y. Wang, R. Bandyopadhyay and P. Pramanik, *New J. Chem.*, 2020, **44**, 1921–1930.
75 J. Shan, R. Li, K. Yan, Y. Zhu and J. Zhang, *Sens. Actuators, B*, 2016, **237**, 75–80.
76 P. A. Pushpanjali, J. G. Manjunatha and M. T. Shreenivas, *ChemistrySelect*, 2019, **4**, 13427–13433.
77 J. M. P. J. Garrido, M. Melle-Franco, K. Strutyński, F. Borges, C. M. A. Brett and E. M. P. J. Garrido, *J. Environ. Sci. Health, Part A: Toxic/Hazard. Subst. Environ. Eng.*, 2017, **52**, 313–319.
78 T. Chen, Y. Liu, J. Lu, J. Xing, J. Li, T. Liu and Q. Xue, *New J. Chem.*, 2019, **43**, 15169–15176.
79 S. W. Carvalho, T. Santana, C. R. Matos, L. P. Costa, E. M. Sussuchi and I. F. Gimenez, *J. Braz. Chem. Soc.*, 2019, **30**, 1266–1275.
80 M. Radičová, M. Behúl, M. Marton, M. Vojs, R. Bodor, R. Redhammer and A. Vojs Staňová, *Electroanalysis*, 2017, **29**, 1612–1617.
81 T. S. H. Pham, P. J. Mahon, G. Lai and A. Yu, *Electroanalysis*, 2018, **30**, 2185–2194.
82 L. V. de Faria, T. P. Lisboa, G. F. Alves, D. M. de Farias, M. A. C. Matos, R. A. A. Muñoz and R. C. Matos, *Electroanalysis*, 2020, **32**, 2266–2272.
83 B. Hatamluyi, F. Modarres Zahed, Z. Es'haghi and M. Darroudi, *Electroanalysis*, 2020, **32**, 1818–1827.
84 R. Rani, A. Deep, B. Mizaikoff and S. Singh, *Electroanalysis*, 2020, **32**, 2442–2451.
85 P. R. Ipte, S. Kumar and A. K. Satpati, *J. Environ. Sci. Health, Part A: Toxic/Hazard. Subst. Environ. Eng.*, 2020, **55**, 142–150.
86 J. V. Kumar, R. Karthik, S.-M. Chen, V. Muthuraj and C. Karuppiah, *Sci. Rep.*, 2016, **6**, 34149.
87 R. R. Sawkar, M. M. Shanbhag, S. M. Tuwar, K. Mondal and N. P. Shetti, *Materials*, 2022, **15**, 7872.
88 S. Bano, A. S. Ganie, R. I. A. Khan, S. Sultana, M. Z. Khan and S. Sabir, *Surf. Interfaces*, 2022, **29**, 101786.
89 N. Chaudhary, A. K. Yadav, J. G. Sharma and P. R. Solanki, *J. Environ. Chem. Eng.*, 2021, **9**, 106771.
90 S. V. Kergaravat, N. Romero, L. Regaldo, G. R. Castro, S. R. Hernández and A. M. Gagneten, *Microchem. J.*, 2021, **162**, 105832.
91 T. Matsunaga, T. Kondo, T. Osasa, A. Kotsugai, I. Shitanda, Y. Hoshi, M. Itagaki, T. Aikawa, T. Tojo and M. Yuasa, *Carbon*, 2020, **159**, 247–254.
92 A. Pollap, K. Baran, N. Kuszewska and J. Kochana, *J. Electroanal. Chem.*, 2020, **878**, 114574.
93 W. D. Adane, B. S. Chandravanshi and M. Tessema, *Sens. Bio-Sens. Res.*, 2023, **39**, 100547.
94 N. M. Umesh, J. A. A. Jesila and S.-F. Wang, *Microchim. Acta*, 2022, **189**, 1–10.

95 L. V. Faria, J. F. Pereira, G. C. Azevedo, M. A. Matos, R. A. Munoz and R. C. Matos, *J. Braz. Chem. Soc.*, 2019, **30**, 1947–1954.
96 A. J. Xie, Y. Chen, S. P. Luo, Y. W. Tao, Y. S. Jin and W. W. Li, *Mater. Technol.*, 2015, **30**, 362–367.
97 S. A. Lim and M. U. Ahmed, *Anal. Sci.*, 2016, **32**, 687–693.
98 H. Chen, L. Bo, M. He, G. Mi and J. Li, *Chem. Lett.*, 2015, **44**, 815–817.
99 X. Zhang, Y. Wei and Y. Ding, *Anal. Chim. Acta*, 2014, **835**, 29–36.
100 H. S. Vedhavathi, B. P. Sanjay, M. Basavaraju, B. S. Madhukar and N. K. Swamy, *J. Electrochem. Sci. Eng.*, 2022, **12**, 59–70.
101 G. S. Garbellini, R. C. Rocha-Filho and O. Fatibello-Filho, *Anal. Methods*, 2015, **7**, 3411–3418.
102 K. Cinková, D. Andrejčáková and Ľ. Švorc, *Acta Chim. Slovaca*, 2016, **9**, 146–151.
103 C. Yan, J. Li, T. Meng, X. Liu, R. Zhang, Y. Chen and G. Wang, *Int. J. Electrochem. Sci.*, 2016, **11**, 6466–6476.
104 G. F. Alves, L. V. de Faria, T. P. Lisboa, M. A. C. Matos and R. C. Matos, *J. Appl. Electrochem.*, 2023, **53**, 39–48.
105 X. Yue, C. Wu, Z. Zhou, L. Fu and Y. Bai, *Foods*, 2022, **11**, 3138.
106 S.-S. Wu, C.-Y. Chein and Y.-H. Wen, *J. Chromatogr. Sci.*, 2008, **46**, 490–495.
107 T. A. Zehra, F. Versiani, M. A. Wahid, S. Jahangir, S. Shah and M. Raza, *Turk. J. Chem.*, 2021, **45**, 1814–1827.
108 C. Grondin, W. Zhao, M. Fakhoury and E. Jacqz-Aigrain, *Biomed. Chromatogr.*, 2011, **25**, 827–832.